A Nuclear Zip Code in *SKS1* mRNA Promotes Its Slow Export, Nuclear Retention, and Degradation by the Nuclear Exosome/DRN in *Saccharomyces cerevisiae*

Subhadeep Das [1], Subir Biswas [3], Shouvik Chaudhuri [2], Arindam Bhattacharyya [3] and Biswadip Das [1]

*1 - **Department of Life Science and Biotechnology,** Jadavpur University, Kolkata, India*
*2 - **Department of Mechanical Engineering,** Jadavpur University, Kolkata, India*
*3 - **Department of Zoology,** University of Calcutta, Kolkata, India*

***Correspondence to Biswadip Das:** Department of Life Science and Biotechnology, Jadavpur University, 188 Raja S.C. Mullick Road, Kolkata 700 032, West Bengal, India. biswadipdas22@gmail.com, biswadip_das@yahoo.com*
https://doi.org/10.1016/j.jmb.2019.07.005

Abstract

In *Saccharomyces cerevisiae*, a special class of mRNAs representing a subset of otherwise normal transcripts displays very slow export and an unusually long intra-nuclear dwell time. This prolonged nuclear retention leads to their rapid degradation in the nucleus by the nuclear exosome and DRN (*D*ecay of *R*NA in the *N*ucleus) apparatus. We previously attributed their slow export to one or more hypothetical *cis*-acting, export-retarding element(s). Here, we identified such a *cis*-element (hereafter referred to as "nuclear zip code") in *SKS1* mRNA, a representative of this class of transcripts. Deletion analysis of *SKS1* mRNA identified a 202-nt RNA segment within the *SKS1* ORF, which harbors the nuclear zip code. Removal of this segment (i) abolished slow export of the transcripts, as revealed by *in situ* confocal microscopy-based localization experiments, and (ii) abrogated the susceptibility of the transcripts to degradation by the nuclear exosome/DRN. Remarkably, fusing the *SKS1* mRNA 202-nt nuclear zip code to the 5′-segment of *CYC1* mRNA resulted in inefficient export, and susceptibility of the chimeric transcript to the nuclear exosome/DRN. These findings identify a *cis*-acting zip code element that is necessary and sufficient to impede nuclear export and results in its preferential nuclear retention, thereby impacting its abundance and cellular repertoire. We conclude that this element posttranscriptionally regulates *SKS1* gene expression levels.

Introduction

Nuclear mRNP biogenesis begins with transcription of protein-coding genes and is followed by a number of processing events, including capping of the nascent transcript at the 5′-end, pre-mRNA splicing, and cleavage/polyadenylation at the 3′-end of the message [1–6]. In addition, each transcript becomes associated with mRNA maturation factors and heterogeneous nuclear ribonucleoproteins [7–12]. mRNP assembly begins with the association of the heterodimeric nuclear cap binding complex (CBC) to the m^7G cap [12] followed by the recruitment of the transcription/export (TREX) complex onto the maturing message. TREX consists of THO proteins (Hpr1p, Mft1p, Tho2p, Thp2p), the mRNA export factor/RNA helicase Sub2p (UAP56 in human), and the RNA binding protein Yra1p (REF/ALY in human) [6,13,14]. Deposition of these proteins onto the nascent transcript facilitates splicing and subsequent association of the transcript with the export receptor Mex67p:Mtr2p (NXF1:p15 in human), various heterogeneous nuclear ribonucleoproteins, and poly(A) tail binding protein Pab1p [7,8]. The collective and concerted action of the whole spectrum of RNA-binding proteins ultimately leads to the formation of mature export-competent mRNPs [14–17]. These mRNPs are released from the site of transcription and move to the nuclear periphery and are exported through nuclear pores to the cytoplasm [1,13,18–21].

Interestingly, transcription and nuclear pre-mRNA processing events are physically and functionally coupled *via* the C-terminal domain of the Rpb1p (the

largest subunit of RNA polymerase II, RNAPII). C-terminal domain acts as a loading platform for transcription and other mRNA processing factors [6,22–27]. Each of the mRNP biogenesis events is thus believed to impact its following step depending on the status of the preceding event(s). This functional interplay was demonstrated to (i) enhance the probability of the formation of export-competent and productive mRNPs and (ii) reduce the possibility of generation of the functionally defective transcripts [23,24,28–31]. Defective mRNPs, however, still generate despite having a tight functional coupling between various mRNP biogenesis events. These faulty messages are rapidly eliminated by a variety of mRNA surveillance and quality control mechanisms [32–40]. In the nucleus of the *Saccharomyces cerevisiae*, a diverse class of aberrant mRNAs undergoes rapid and selective degradation by the nuclear exosome in association with TRAMP and DRN [2,36,40–46]. These faulty mRNAs include the transcription elongation assembly-defective transcripts [47–53], intron-containing splice-defective messages [54–56], transcription termination-defective 3′-extended read-through transcripts [57,58], and export-defective mRNAs [46,59,60]. The nuclear exosome consists of nine catalytically inactive (Rrp4p, Rrp40p, Csl4p, Rrp41p, Rrp42p, Rrp43p, Rrp45p, Rrp46p, and Mtr3p) and two functionally active (Dis3p/Rrp44 and Rrp6p) subunits, and a few associated nuclear and cytoplasmic cofactors [41,44,59,61–67]. However, the exosome requires assistance from the ancillary co-factors to correctly select and target faulty transcripts. These co-factors stimulate exosome function as well as helping it to selectively target aberrant mRNPs [33]. TRAMP (*TR*f4p/5p-*A*ir1p/2p-*M*tr4p *P*olyadenylation Complex) in *S. cerevisiae* is a well-characterized example of ancillary complex, which consists of DExH box RNA helicase, Mtr4p, non-canonical poly (A) polymerase, Trf4p (Pap2p)/Trf5p, and Zn-knuckle RNA binding proteins, Air1p/2p [33,44,68,69]. In addition, DRN defines a nuclear mRNA decay

Table 1. List and genotypes of yeast strains used in this study

Strain no.	Complete genotype	Reference
yBD 5	*MATa cyc1-512 ura3-52 trp2-1*	[57]
yBD 6	*MATa cyc1-512 cbc1::URA3 ura3-52 trp2-1*	[57]
yBD 58	*MATa his3-Δ1 leu2-Δ0 lys2-Δ0 ura3-Δ0*	[60]
yBD 456	*MATa cyc1-512 ura3-52 trp2-1 sks1-Δ*	This work[a]
yBD 457	*MATa cyc1-512 ura3-52 trp2-1 sks1-Δ cbc1-Δ::hisG*	This work[a]
yBD 358	*MATa cyc1-512 ura3-52 trp2-1 sks1-Δ::SKS1-N-Δ1 cbc1-Δ::hisG*	This work[a]
yBD 359	*MATa cyc1-512 ura3-52 trp2-1 sks1-Δ:: SKS1-N-Δ2*	This work[a]
yBD 360	*MATa cyc1-512 ura3-52 trp2-1 sks1-Δ::SKS1-N-Δ2 cbc1-Δ::hisG*	This work[a]
yBD 361	*MATa cyc1-512 ura3-52 trp2-1 sks1-Δ:: SKS1-N-Δ3*	This work[a]
yBD 362	*MATa cyc1-512 ura3-52 trp2-1 sks1-Δ::SKS1-N-Δ3 cbc1-Δ::hisG*	This work[a]
yBD 363	*MATa cyc1-512 ura3-52 trp2-1 sks1-Δ::SKS1-N-Δ4*	This work[a]
yBD 364	*MATa cyc1-512 ura3-52 trp2-1 sks1-Δ::SKS1-N-Δ4 cbc1-Δ::hisG*	This work[a]
yBD 365	*MATa cyc1-512 ura3-52 trp2-1 sks1-Δ::SKS1-N-Δ5*	This work[a]
yBD 366	*MATa cyc1-512 ura3-52 trp2-1 sks1-Δ::SKS1-N-Δ5 cbc1-Δ::hisG*	This work[a]
yBD 458	*MATa cyc1-512 ura3-52 trp2-1 sks1-Δ::SKS1-N-Δ6*	This work[a]
yBD 459	*MATa cyc1-512 ura3-52 trp2-1 sks1-Δ::SKS1-N-Δ6 cbc1-Δ::hisG*	This work[a]
yBD 460	*MATa cyc1-512 ura3-52 trp2-1 sks1-Δ::SKS1-N-Δ7*	This work[a]
yBD 461	*MATa cyc1-512 ura3-52 trp2-1 sks1-Δ::SKS1-N-Δ7 cbc1-Δ::hisG*	This work[a]
yBD 462	*MATa cyc1-512 ura3-52 trp2-1 sks1-Δ::SKS1-N-Δ1*	This work[a]
yBD 463	*MATa cyc1-512 ura3-52 trp2-1 sks1-Δ::SKS1-N-Δ2 rrp6-Δ::URA3*	This work[a]
yBD 464	*MATa cyc1-512 ura3-52 trp2-1 sks1-Δ::SKS1-N-Δ6 rrp6-Δ::URA3*	This work[a]
yBD 465	*MATa cyc1-512 ura3-52 trp2-1 sks1-Δ::SKS1-N-Δ5 rrp6-Δ::URA3*	This work[a]
yBD 466	*MATa cyc1-512 rrp6::URA3 ura3-52 trp2-1*	This work[a]
yBD 467	*MATa ura3-52 trp2-1 sks1-Δ*	This work[a]
yBD 468	*MATa cyc1::CYC1 ura3-52 trp2-1 sks1-Δ*	This work[a]
yBD 469	*MATa cyc1::ΔCYC1 ura3-52 trp2-1 sks1-Δ*	This work[a]
yBD 470	*MATa cyc1:: CYC1-SKS1-ch ura3-52 trp2-1 sks1-Δ*	This work[a]
yBD 471	*MATa his3-Δ1 leu2-Δ0 lys2-Δ0 ura3-Δ0 pBD56 pBD72*	This work[a]
yBD 472	*MATa his3-Δ1 leu2-Δ0 lys2-Δ0 ura3-Δ0 pBD56 pBD286*	This work[a]
yBD 473	*MATa his3-Δ1 leu2-Δ0 lys2-Δ0 ura3-Δ0 pBD56 pBD287*	This work[a]
yBD 474	*MATa his3-Δ1 leu2-Δ0 lys2-Δ0 ura3-Δ0 pBD56 pBD57*	This work[a]
yBD 485	*MATa cyc1::CYC1-NZ ura3-52 trp2-1 sks1-Δ*	This work[a]
yBD 486	*MATa cyc1:: CYC1 ura3-52 trp2-1 sks1-Δ cbc1-Δ::hisG*	This work[a]
yBD 487	*MATa cyc1:: CYC1 ura3-52 trp2-1 sks1-Δ rrp6-Δ::URA3*	This work[a]
yBD 488	*MATa cyc1::ΔCYC1 ura3-52 trp2-1 sks1-Δ cbc1-Δ::hisG*	This work[a]
yBD489	*MATa cyc1:: ΔCYC1 ura3-52 trp2-1 sks1-Δ rrp6-Δ::URA3*	This work[a]
yBD490	*MATa cyc1:: CYC1-NZ ura3-52 trp2-1 sks1-Δ cbc1-Δ::hisG*	This work[a]
yBD491	*MATa cyc1:: CYC1-NZ ura3-52 trp2-1 sks1-Δ rrp6-Δ::URA3*	This work[a]

[a] Constructed in the laboratory during the period of work.

apparatus that consists of nuclear mRNA-cap binding protein, Cbc1p/2p [57,70], Rrp6p [62], and two nucleocytoplasmic shuttling proteins, Upf3p and Tif4631p [70]. Previous genetic data and a body of recent findings indicate that DRN assists the nuclear exosome to selectively degrade aberrantly long 3′-extended and export-defective messages [46].

Strikingly, the abundance and stability of approximately two hundred normal mRNAs were previously found to be enhanced in both *cbc1*-Δ and *rrp6*-Δ yeast strains from transcriptomic analyses [60]. Findings from these experiments supported the argument that nuclear exosome in association with DRN acts on these otherwise normal mRNAs to control their physiological levels by preferential mRNA decay [60]. This special class of mRNAs includes *SKS1*, *IMP3*, *YLR194c*, *HAC1*, *RPB11*, and *YBR259w* [60]. Genetic and cytological analysis suggested that the slow export of some of these messages resulted in their susceptibility to the exosome/DRN. We subsequently proposed the existence of a "kinetic competition" between the nuclear export of mRNA and nuclear degradation to explain their susceptibility to exosome/DRN [60]. In this view, slow export plays a critical role in determining if a transcript is subject to exosome/DRN action [60]. However, the mechanistic basis for this phenomenon remains unclear.

We postulated that these transcripts are exposed to DRN by virtue of *cis*-acting elements that slow their nuclear export. To identify these sequences, we studied *SKS1* mRNA, which is slowly exported from the nucleus and degraded by DRN [60]. *SKS1* encodes a putative serine/threonine protein kinase that serves as a multi-copy suppressor of *snf3*-Δ yeast strain [71], which is unable to grow in low-glucose medium because of a defect in the high-affinity glucose transport [72].

Our results reveal that slowed nuclear export and the exosome/DRN-dependent degradation of *SKS1* mRNA require a 202-nt-long RNA segment, or nuclear zip code, within the *SKS1* ORF. Moreover, the zip code is sufficient to retard the nuclear export of a chimeric mRNA that was constructed by fusing the nuclear zip code to the 5′-segment of the stable *CYC1* mRNA and subsequently promote its decay by the exosome/DRN. Our findings thus identify an mRNA zip code that is necessary and sufficient to slow nuclear export and target-specific transcripts for DRN.

Results

The physiological abundance of the *SKS1* mRNA relies on the presence of a specific segment of its transcript body

We asked if the elimination of specific sequences in the *SKS1* transcript would facilitate its rapid

Table 2. List and descriptions of plasmids used in this study

Plasmid no.	Description	Reference
pBD 56	p*GAL–U1A* (1–94)—*GFP*, *LEU2* fusion gene under galactose control cloned in pRS315	[73]
pBD 57	*pGK1–PGK1–U1As–ASH1* 3′ UTR-ADH1 terminator in pRS426, URA3	[73]
pBD 72	2.5 kb XhoI–BamHI *SKS1* coding region and 1kb upstream replacing *PGK1* in pAB 3123	[60]
pBD 286	1.8 kb (33–682 bp deleted from ORF) XhoI–BamHI *SKS1* coding region and 1 kb upstream replacing *PGK1* in pAB 3123	This work[a]
pBD 287	2.3 kb (825–1026 bp deleted from ORF) XhoI–BamHI *SKS1* coding region and 1kb upstream replacing *PGK1* in pAB 3123	This work[a]
pBD 288	650 bp of *SKS1* ORF (33–682 bp) has been deleted from pRS 306 *SKS1* by reverse PCR using primer pair OBD 111 and OBD 112. Host cell: XL1 blue	This work[a]
pBD 289	948 bp of *SKS1* ORF (78–1025 bp deleted from *pUC19 SKS1* using restriction enzymes pair PflMI and ApaI) subcloned into *pRS306* using HindIII and SacI. Host cell: *Escherichia coli* DH5α	This work[a]
pBD 290	743 bp of *SKS1* ORF (78–824 bp deleted from pUC 19 *SKS1* using restriction enzymes pair PflMI and NcoI) subcloned into pRS306 using HindIII and SacI. Host cell: *E. coli* DH5α	This work[a]
pBD 291	503 bp of *SKS1* ORF (1023–1525 bp) has been deleted from pRS 306 *SKS1* by reverse PCR using primer pair OBD 298 and OBD 299. Host cell: *E. coli* DH5α	This work[a]
pBD 292	833 bp of *SKS1* ORF (669–1501 bp) has been deleted from pRS 306 *SKS1* by reverse PCR using primer pair OBD 292 and OBD 293. Host cell: One shot	This work[a]
pBD 223	202 bp of *SKS1* ORF (825–1026 bp deleted from pUC 19 *SKS1* by ApaI and NcoI) subcloned into pRS306 using HindIII and SacI. Host cell: *E. coli* DH5α	This work[a]
pBD 253	301 bp of SKS1 ORF (1025–1325 bp deleted from pRS 306 SKS1 by reverse PCR using OBD 299 and OBD 333. Host cell: Host cell: *E. coli* DH5α	This work[a]
pBD 252	A 2.7 kb SacI/XbaI fragment of *CYC1* gene inserted in the SacI/XbaI site of pRS 306. Host cell: *E. coli* DH5α	This work[a]
pBD 293	100 bp of *CYC1* ORF (231–330 bp) has been deleted from pRS 306 *SKS1* by reverse PCR using primer pair OBD 567 and OBD 569. Host cell: *E. coli* DH5α	This work[a]
pBD 295	202 bp of *SKS1* ORF has been cloned in pBD293 by using restriction enzyme SmaI. Host cell: *E. coli* DH5α	This work[a]

[a] Constructed in the laboratory during the period of work.

Table 3. Oligonucleotides used for end point PCR in this study

Name	Sequence	Used in the
OBD111 To prepare SKS1 deletion constructs. This work¥	5′ CGACCCTATTTGAGCCGTTA 3′	Construction of *SKS1* deletion
OBD112	5′ TTTGAATACCACCACCAACG 3′	Construction of *SKS1* deletion Construction of *CYC1-NZ* chimeric gene
OBD298	5′ GCAGGTCTCACCTTTATACTCACT 3′	Construction of *SKS1* deletion
OBD299	5′ CCCTTCCCTGGTGAAAGAAGT 3′	Construction of *SKS1* deletion
OBD292	5′ CCACCAGAGAAATGGTTACCAGA 3′	Construction of *SKS1* deletion
OBD293	5′ GAACTGCCAACGCACACATT 3′	Construction of *SKS1* deletion
OBD333	5′-TGACGGAAGTATGGAAAAGTATGAAT 3′	Construction of *SKS1* deletion
OBD109	5′ CAGTGATCTAATGCGGAGCA 3′	Quantification of *SKS1* mRNA by qRT-PCR analysis
OBD110	5′ CTCTTCTGCAAACGCAACTG 3′	Quantification of *SKS1* mRNA by qRT-PCR analysis
OBD311	5′ TACAAAACCAGGAACAAGCACAA 3′	Quantification of *SKS1* mRNA by qRT-PCR analysis
OBD117	5′ TGAGACCTGCTCAATAATCTGG 3′	Construction of *CYC1-NZ* chimeric gene and its sequencing
OBD331	5′ CCTTTTTAACTTCCTCAATGGACAGT 3′	Quantification of *SKS1* mRNA by qRT-PCR analysis
OBD332	5′ CAATCTTTGGAAGCACTAACGTCAT 3	Quantification of *SKS1* mRNA by qRT-PCR analysis
OBD274	5′ CCTACTGGATCGCAATGACAAC-3′	Quantification and sequencing of *SKS1* deletion construct
OBD275	5′ CGCACACATTTGGAGCTAGATATT-3′	Quantification of *SKS1* mRNA by qRT-PCR analysis
OBD9	5′ ACGATAGCG GATGCGCTGGG 3′	Quantification and sequencing of *SKS1* deletion construct
OBD10	5′ TCACTCTCCGGTTCAGCATCTTCC3′	Sequencing of *SKS1* deletion construct
OBD249	5′ CTTGCCCGACCTTGTGCTAT 3′	Sequencing of *SKS1* deletion construct
OBD288	5′ GCAGCTTTGCTCCGCATTAG 3′	Sequencing of *SKS1* deletion construct
OBD567	5′ CCCTTTTCCTTTGTCGATATCAT3′	Construction of *CYC1-NZ* chimera and Δ*CYC1* deletion
OBD569	5′ GGTTAGTCAAGTACTCTGACATG 3′	Construction of *CYC1-NZ* chimera and Δ*CYC1* deletion
OBD475	5′ GGGCTCGAGCTGTACTCTATGTACA 3′	Construction of *SKS1* deletion fluorescence constructs
OBD476	5′ TAAGAGGATCCAGTGAGTATAAAGGTGAG-3′	Construction of *SKS1* deletion fluorescence constructs
OBD1	5′ TTTGGCTCCATATGATCACTAC 3′	Quantification of *LYS2* mRNA by qRT-PCR analysis
OBD2	5′ TTTGTAACGTTAGACAATCACG 3′	Quantification of *LYS2* mRNA by qRT-PCR analysis
OBD262	5′ ATCCCGTTAGCTTCCAGGC 3′	Quantification of *RNA15* mRNA by qRT-PCR analysis
OBD263	5′ CCATCCTTTCATCATCGGGC 3′	Quantification of *RNA15* mRNA by qRT-PCR analysis
OBD176	5′ ATTTACTGAATTAACAATGGATTC 3′	Quantification of *ACT1* mRNA by qRT-PCR analysis
OBD177	5′ GGCAACTCTCAATTCGT 3′	Quantification of *ACT1* mRNA by qRT-PCR analysis
OBD268	5′ GCCGAAAGAATGCAAAAGGA 3′	Quantification of *ACT1* mRNA by qRT-PCR analysis
OBD269	5′ TCTGGAGGAGCAATGATCTTGA 3′	Quantification of *ACT1* mRNA by qRT-PCR analysis
OBD272	5′ GTGTGGATTTGATGGTATGTGTGA 3′	Quantification of *LYS2* mRNA by qRT-PCR analysis
OBD273	5′ GATATGCAGGGTCGATAACTGAAA 3′	Quantification of *LYS2* mRNA by qRT-PCR analysis
OBD186	5′ AATTCAAGGCCGGTTCTGCT 3′	Quantification and sequencing of *CYC1* deletion construct
OBD588	5′ ACGGTGTGGCATTGTAGACATC 3′	Quantification of *CYC1* mRNA by qRT-PCR analysis
OBD233	5′ CGATGACGTTAGTGCTTCCA	Detection of poly(A) tail of *SKS1* deletion constructs
OBD290	5′-TGCAGCTTTGCTCCGCATTA-3′	Detection of poly(A) tail of *SKS1* deletion constructs
OBD392	5′-GCGAGCTCCGCGGCCGCGTTTTTTTTTTT-3′	Adapter oligo-deoxynucleotide used in the LM-PAT reaction for the detection of poly(A) tail of *SKS1* full-length and deletion messages, *ACT1* and *CYH2* mRNAs
OBD395	5;′-CCATGAAGGTCAAGATCATTGCTCCTCCA-3′	Gene specific primer for *ACT1*, used in LM-PAT PCR reaction for the detection of poly(A) tail *ACT1* mRNA
OBD396	5′-CCCAGAAGACAAGAGAGACCAATACTTG-3′	Detection of poly(A) tail of *CYH2* mRNA
OBD648	5′-GTGTACAAATGCTGTCAGACT-3′	Complimentary to the 5′-UTR of *SKS1* mRNA, quantification of *SKS1* mRNA by qRT-PCR analysis
OBD649	5′-TTATGTTCTAATTCGGTAATAGCTTCA-3′	Complimentary to the 3′-UTR of *SKS1* mRNA, quantification of *SKS1* mRNA by qRT-PCR analysis

αProcured in the laboratory during the period of work.

nuclear export and suppress its degradation by the nuclear exosome/DRN. Consequently, we constructed a series of deletion mutants that lack various portions of its transcript body (Fig. 1A, Table 4). Since, no information about the length of the 5′- and 3′-UTR of the *SKS1* message was available, we first mapped the 5′- and 3′-end of this RNA by 5′-RACE-PCR and LM-PAT [74] assays, respectively, as described in the Materials and Methods section. Cloning and sequencing of the 5′-RACE products revealed two transcription start points: the major one is located at 67 nt upstream, and the minor one is located at 46 nt upstream, with respect to the initiator AUG codon (Fig. 1A). LM-PAT assay (see next section) suggested that the 3′-UTR of this message consists of 76 nt, 3′ to the terminator UGA codon (Fig. 2D). This information defined the physical boundary of the *SKS1* mRNA and enabled

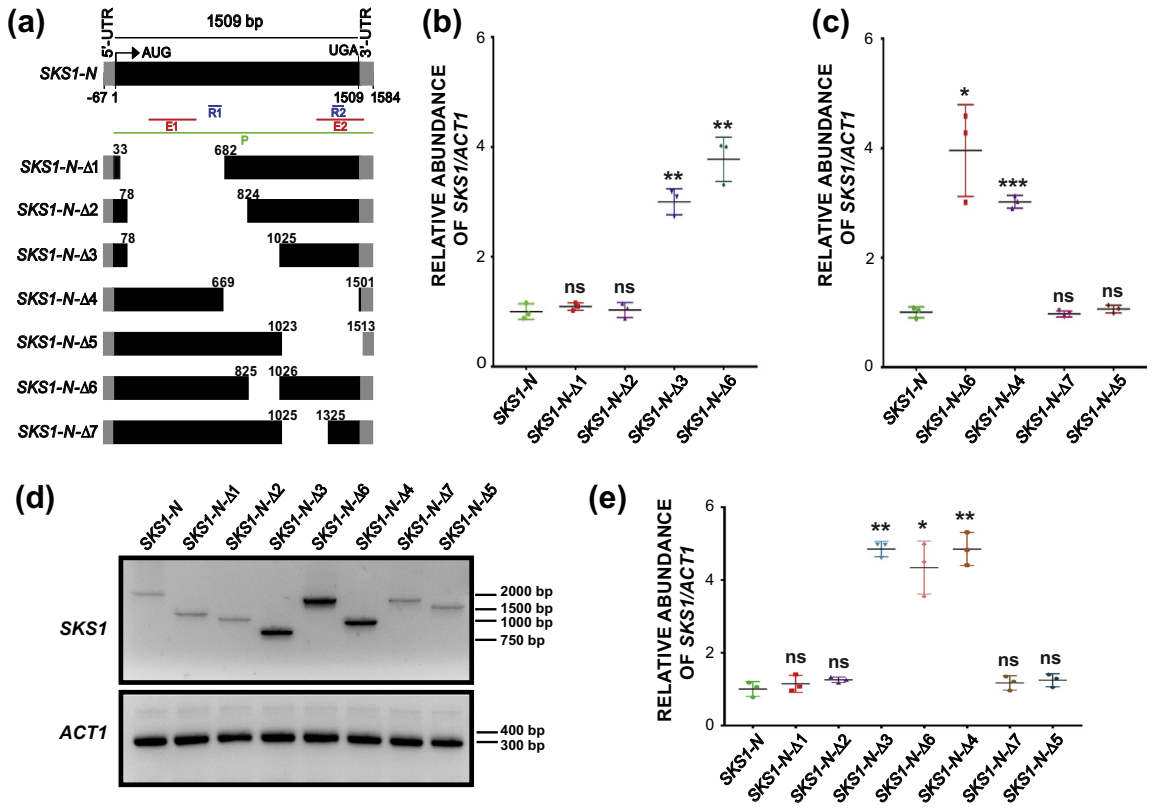

Fig. 1. A nuclear zip code element dictates the cellular abundance of *SKS1* message. (A) Schematic presentation of *SKS1* mRNA (*SKS1-N*, N stands for the native and full-length mRNA) and the various deletion constructs of this mRNA used in this study. The ORF of the full-length mRNA and start and stop sites are indicated. The ORF is flanked by a 67-nt-long 5′- and a 76-nt-long 3′-UTR, whose coordinates [numbered with reference to the AUG codon (+1)] are indicated at the bottom. Each deletion in the *SKS1* transcript body is designated by a specific allele number (*SKS1-N-Δ1* through *SKS1-N-Δ7*). Various amplicons used to either detect the full-length/deleted *SKS1* mRNAs or quantify their abundance are indicated in different colors below the cartoon of the full-length *SKS1* mRNA: R1 and R2 (blue) amplicons were used for qRT-PCR, whereas E1, E2 (red), and P (green) amplicons were used in end-point and semi-quantitative PCR reactions. (B–C) Scatter plot obtained from the qRT-PCR analysis revealing the relative levels of full-length *SKS1* mRNA (*SKS1-N*) and its deleted versions (*SKS1-N*-Δ1, *SKS1-N*-Δ2, *SKS1-N*-Δ3, and *SKS1-N*-Δ6 shown in panel B, and *SKS1-N*-Δ6, *SKS1-N*-Δ4, *SKS1-N*-Δ7, and *SKS1-N*-Δ5 shown in panel C) in a normal (yBD-5) strain using random oligomer-primed cDNA samples made from the indicated strains with a primer set encompassing either the amplicon R2 (for panel B) or the amplicon R1 (for panel C) (shown in Fig. 1A). For both the experiments presented in Fig. 1B and C, three independent random oligomer-primed cDNA preparations (biological replicates, $n = 3$) for each sample were used to determine the levels of *SKS1* and *ACT1* mRNAs. Normalized values of *SKS1* mRNA with respect to *ACT1* signal in the yeast strain harboring the *SKS1-N* allele were set to 1. The statistical significance of difference as reflected in the ranges of *P* values estimated from Student's two-tailed *t* tests for a given pair of test strains for each message is presented with the following symbols, *<0.05, **<0.005, and ***<0.001; ns, not significant. (D) Representative gel showing the sizes and the relative levels of full-length *SKS1* transcript-body (excluding polyA tail), and its various deleted versions determined from semi-quantitative end-point PCR using random-oligomer-primed cDNA samples with a primer set encompassing the amplicon P (shown in Fig. 1A). The bottom panel shows the relative levels of *ACT1* message in these strains. (E) Scatter plot presenting the relative levels of full-length/deleted *SKS1* messages in the normal yeast strain as determined from the signals associated with the bands in the panel 1D (determined as described in Materials and Methods). Three independent random oligomer-primed cDNA preparations (biological replicates, $n = 3$) were used to determine the levels of full-length/deleted *SKS1*messages and *ACT1* mRNAs in the same samples. Normalized values of each of the *SKS1* with respect to *ACT1* signal in the yeast strain harboring the *SKS1-N* allele were set to 1. The statistical significance of difference as reflected in the ranges of *P* values is presented with the following symbols, *<0.05, **<0.005, and ***<0.001; ns, not significant.

us to design the deletion constructs in a precise manner.

Next, we constructed a series of deletion mutants of this RNA using a combination of reverse PCR and restriction digestion (Fig. 1A, Table 4). To avoid the copy number variations among different constructs (which in turn may affect the abundance of the corresponding transcript levels), the native full-length *SKS1* gene (denoted *SKS1-N*) and all the deletion constructs were integrated into the genomic

Table 4. List of deletion scheme used in this study

Construct identity	Length of the deletion (in bp)	Span of the deletion with respect to *SKS1* ORF (in bp)	Susceptibility to the nuclear exosome/DRN and putative *in situ* localization	Length of poly(A) tail (as determined from LM-PAT data)	Constructed by	Primers/ enzymes used
SKS1-N-Δ1	650	33 to 682	Susceptible, nuclear	≈165 nt	Reverse PCR	oBD 111 oBD 112
SKS1-N-Δ2	743	78 to 824	Susceptible, nuclear	≈165 nt	Digestion by restriction enzyme	PflMI and ApaI
SKS1-N-Δ3	948	78 to 1025	Insensitive, cytoplasmic	≈165 nt	Digestion by restriction enzyme	PflMI and NcoI
SKS1-N-Δ4	833	669 to 1501	Insensitive, cytoplasmic	≈165 nt	Reverse PCR	oBD 292 oBD 293
SKS1-N-Δ6	202	825 to 1026	Insensitive, cytoplasmic	≈165 nt	Digestion by restriction enzyme	ApaI and NcoI
SKS1-N-Δ7	301	1025 to 1325	Susceptible, nuclear	≈165 nt	Reverse PCR	oBD 299 oBD 333
SKS1-N-Δ5	490	1023 to 1513	Susceptible, nuclear	≈165 nt	Reverse PCR	oBD 298 oBD 299
SKS1-U-Δ1	650	33 to 682	Susceptibility, not determined, nuclear	ND	Reverse PCR technology	oBD 111 oBD 112
SKS1-U-Δ6	202	825 to 1026	Susceptibility, not determined, cytoplasmic	ND	Digestion by restriction enzyme	ApaI and NcoI
Δ*CYC1*	100	231 to 330	Insensitive, cytoplasmic	ND	Reverse PCR technology restriction	oBD 567 oBD 569
5′-CYC1-NZ	Not Applicable	3′-202 bp of *SKS1* fused to 5′-230 bp of *CYC1*	Susceptible, nuclear	ND	Digestion by restriction enzyme and ligation	SmaI

bp, base-pair; ND, not determined.

SKS1 locus by two-step gene replacement procedure in a yeast strain carrying the complete deletion of the endogenous *SKS1* ORF. In order to compare the abundance of the resulting transcripts with that of the full-length native transcripts, their steady-state levels were determined using both the end-point and quantitative RT-PCR. Since, different segments were removed from the *SKS1* ORF in various constructs, two sets of primer pairs were used for qRT-PCR and end-point PCR reactions in order to analyze the cellular abundance of the deleted transcripts, since the binding sites of a specific primer pair on all the constructs were not available (refer to Fig. 1A). To measure the relative steady-state levels of *SKS1-N*-Δ1, *SKS1-N*-Δ2, *SKS1-N*-Δ3, and *SKS1-N*-Δ6 with respect to *SKS1-N* message, the primer pairs oBD331/332 (used in qRT-PCR analyses, encompassing the amplicon R2, Fig. 1A) and oBD311/117 (used in end-point PCR, encompassing the amplicon E2, Fig. 1A) were used. The relative steady-state levels of *SKS1-N*-Δ6, *SKS1-N*-Δ4, *SKS1-N*-Δ7, and *SKS1-N*-Δ5 with respect to *SKS1-N* message, in contrast, were determined using the primer-pairs oBD274/275 (used in qRT-PCR analyses, encompassing the amplicon R1, Fig. 1A) and oBD109/110 (used in end-point PCR, encompassing the amplicon E1, Fig. 1A).

Both qRT-PCR and end-point PCR (data not shown) assays revealed that the steady-state levels of *SKS1-N*-Δ1, *SKS1-N*-Δ2, *SKS1-N*-Δ7, and *SKS1-N*-Δ5 are very similar to the full-length native *SKS1-N* transcript (Fig. 1B–C). Interestingly, the levels of *SKS1-N*-Δ3, *SKS1-N*-Δ4, and *SKS1-N*-Δ6 transcripts, in contrast, increased 3- to 4-fold compared to that of the full-length native *SKS1-N* transcript (Fig. 1B–C) as shown in the scatter plots presented in the Fig. 1B and C generated from the qRT-PCR data using the primer sets encompassing the amplicons R1/R2. Remarkably, the relative enhancement of *SKS1-N*-Δ6 transcript level as compared to full-length *SKS1-N* message turned out to be similar (approximately four-fold) using both the amplicons R1 and R2 (note that this deletion message has the binding sites for both the primer pairs) (scatter plots in Fig. 1B–C). This observation thus reflected the validity of our qRT-PCR assay method and justified the method of comparison of the relative level data of full-length *SKS1* mRNA and its various deletion versions obtained using two different primer sets. The combined results suggest that a segment encompassing from 825 to 1026 nt of the *SKS1* transcript plays a critical role in determining the cellular steady-state level of the *SKS1* mRNA.

Next, we asked if the lengths/sizes of transcripts corresponding to each of the deletion mutants are in agreement with the predicted sizes generated by reverse PCR and restriction digestion. It should be

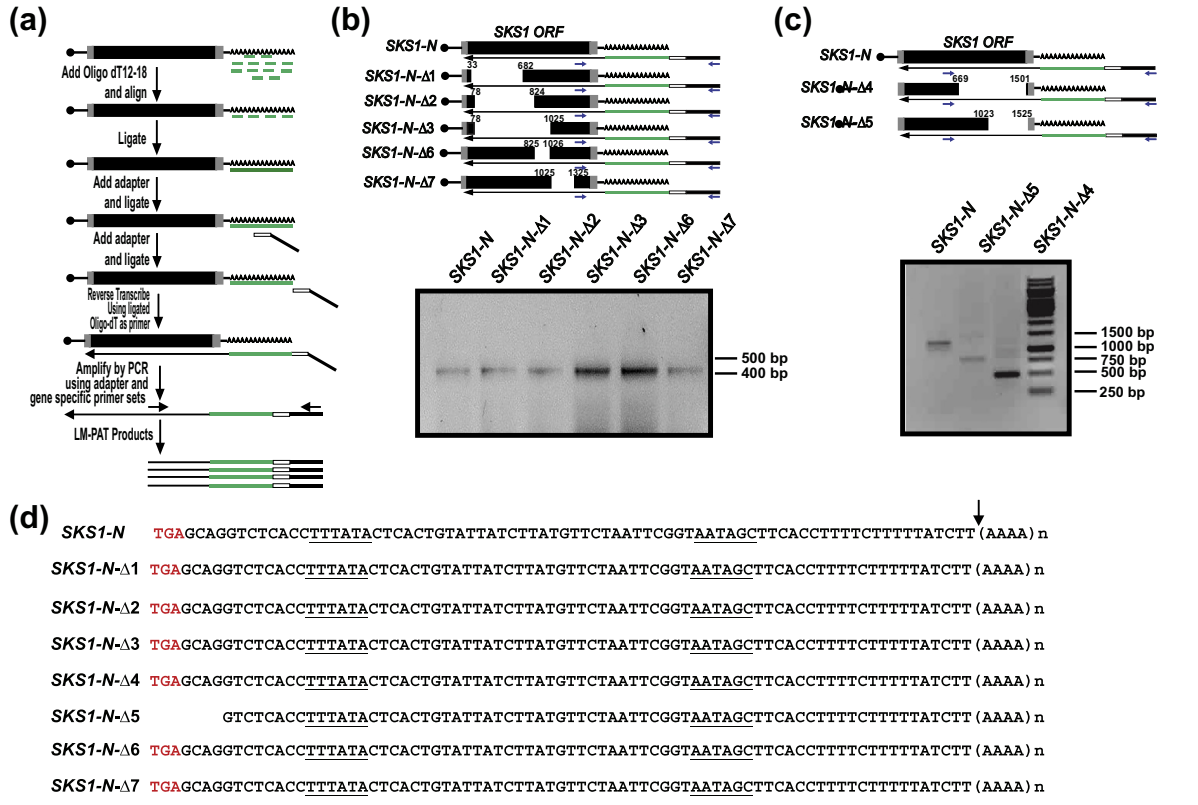

Fig. 2. Deletions at the various locations in the *SKS1* message altered neither the site of polyadenylation nor the length of the poly(A) tail. (A) Schematic showing the steps involved in ligation-mediated poly-A tail (LM-PAT) assay. Mixture of oligo-$dT_{12\text{-}18}$ (indicated by segmented green boxes) was mixed and allowed to align to the poly(A) tails of the total RNAs, which was followed by the ligation of the oligonucleotides at 42 °C. An adapter (consisting of a small segment of oligo-dT and a unique sequence in tandem) was then ligated to the 5′-end of the ligated oligo-dt tail. The ligated adapter-oligo-dT was used as a primer for the first strand cDNA synthesis followed by the PCR amplification of the entire length of the poly (A) tail and 3′-UTR of a specific message. The primer sets used for the PCR consist of a sense primer that is complimentary to a specific region within the ORF and an antisense primer, which is complimentary to the unique region of the adapter (shown in black arrowheads). (B–C) Representative gels showing the length and relative abundance (qualitatively) of the LM-PAT products derived from the full-length and various deleted versions of *SKS1* mRNA resolved in 2% agarose gel. Cartoons presented above each gel panel depict the location of the sense/antisense primer sets (in blue) that yielded a 415-bp product for the full-length and all the selected deleted version of *SKS1* messages (in panel B) and a 1297-, 795-, and 465-bp products for the full length *SKS1-N*, *SKS1-N*-Δ5, and *SKS1-N*-Δ4 deleted messages respectively (in panel C). (D) Alignment of the sequence of the 3′-UTR of the full-length and various deleted versions of the *SKS1* mRNA showing the location of translation stop codon TGA (in red), putative efficiency and positioning elements (underlined), and the actual cleavage/polyadenylation site (downward arrowhead). Note that, while the sequence of the 3′-UTR and the cleavage/polyadenylation site was verified by sequencing of the three independent clones of the LM-PAT products of each construct, the efficiency and positioning elements were not experimentally validated.

noted here that all the deletion clones corresponding to each of the constructs were analyzed and validated by restriction digestion and DNA sequencing prior to their integration into the genome. To address this issue, we carried out a semi-quantitative RT-PCR analysis of the full-length *SKS1* message and its various deletion mutants using a primer set specific to 5′- and 3′-UTR, oBD648/649 encompassing the amplicon P (as shown in Fig. 1A). In order to ensure the linearity of the PCR assay, we carefully monitored the cycle numbers used in this reaction. As shown in Fig. 1D, the sizes corresponding to the signals (bands) associated with the full-length *SKS1* and all the deletion mutants matched perfectly with the predicted sizes (Fig. 1D, Table 4). Moreover, quantification analyses (Fig. 1E) (as described in Materials and Methods) indicated that normalized values (with respect to *ACT1*) of their abundance/relative levels (with respect to the full-length *SKS1* transcript) were also in good agreement with their relative levels obtained from qRT-PCR analyses (Fig. 1D).

These findings strongly indicate that a 202-nt segment corresponding to 825–1026 nt of the *SKS1* mRNA appears to regulate the steady-state levels of the *SKS1* mRNA, possibly by slowing nuclear mRNA

export and targeting the transcript for the exosome/DRN. Note that the steady-state levels of two other arbitrarily chosen typical mRNAs, *RNA15* and *LYS2*, remained unaltered in these isogenic strains harboring the deletions in *SKS1* mRNA (Supplementary Fig. S1D–E). We call this 202-nt *cis*-acting sequence the nuclear zip code (*NZ*) element throughout this manuscript.

Polyadenylation status of the full-length and various deletion mutants of *SKS1* mRNA remained identical

The nuclear exosome targets aberrant messages for degradation in the nucleus, due to poly(A) tail length defects [73,75–79]. Thus, we asked if the low cellular abundance of full-length *SKS1* mRNAs and those deletion mutants *SKS1-N*-Δ1, *SKS1-N*-Δ2, *SKS1-N*-Δ7, and *SKS1-N*-Δ5 messages is attributable to their shorter poly(A) tail. We determined the polyadenylation status of the full-length *SKS1* mRNA and all of the deletion mutants using LM-PAT (*L*igation-*M*ediated-*P*oly(*A*)-*T*ail) assay (Fig. 2A) [73]. We used two different sets of gene-specific sense primers whose relative locations are shown in Fig. 2B and C. For the deletion mutants *SKS1-N*-Δ1, *SKS1-N*-Δ2, *SKS1-N*-Δ3, *SKS1-N*-Δ6, and *SKS1-N*-Δ7, we used oBD233 as the sense primer and adapter as the anti-sense primer, oBD392 (location shown in Fig. 2B) in the final PCR reaction. This reaction yielded a 415-bp product for the full-length *SKS1* and all of the deletion mutants mentioned above (Fig. 2B, bottom panel). For the mutants *SKS1-N*-Δ4 and *SKS1-N*-Δ5, we carried out the PCR using a different sense primer, oBD290 and the same anti-sense primer (location is shown in the cartoon of Fig. 2C) since these two mutants lack the binding site for the previous sense primer (because of the deletion). The LM-PAT products of the full-length *SKS1*, *SKS1-N*-Δ4, and *SKS1-N*-Δ5 deletion mutants consisted of 1297, 465, and 795 bp, respectively (lower panel in Fig. 2C). Subsequent sequencing of all of these products revealed that the 3′-UTR of the full-length *SKS1* and all other deletion versions (except for *SKS1-N*-Δ5 message, whose 3′-UTR lacks the first 4 nt from the 5′-side, see Fig. 2D) are identical in length (76 bp) and sequence (shown in Fig. 2D).

Further analyses demonstrated that (i) the cleavage site, where the polyadenylation starts, remained unaltered in all of these deleted messages (shown with downward arrowhead in Fig. 2D) and (ii) the average length of the poly(A) tail of the normal and all the deleted messages is approximately 160–175 nt long (Table 4). It is interesting to note here that although the average length of the poly(A) tails of the majority of the yeast messages varies between 70 and 90 adenylate residues [80–82], *SKS1* mRNA displayed a much longer poly(A) tail. To validate our LM-PAT assay, we further determined the length of the poly(A) tails of two well-characterized messages, *CYH2* and *ACT1*, in the same yeast strain using our assay system (Supplementary Fig. S2B). The data revealed that the average lengths of the poly(A) tails of these two messages are ≈74 and ≈65 nt, respectively, which lies well within the normal range of 70–90 residues long. These data therefore clearly validated the precision of our assay method and indicated that neither the length of the poly(A) tail nor the cleavage/polyadenylation sites of the full-length and mutant *SKS1* messages were altered, thereby ruling out the possibility that insufficient polyadenylation status of the *SKS1* deletion mutant transcripts might play a role in their observed relative abundance.

The nuclear zip code element of *SKS1* mRNA stimulates its intra-nuclear degradation mediated by the nuclear exosome/DRN

The existence of a “kinetic competition” between nuclear export and the degradation by the exosome/DRN [60,62] leads to a logical corollary that if a given unstable mRNA is exported rapidly, that message would escape the action of the exosome/DRN and thereby would regain its stability. Consequently, after demonstrating that the abundance of *SKS1* mRNA is regulated by a nuclear zip code in its transcript body, we asked if the elimination of the zip code from the *SKS1* transcript body would convert this exosome/DRN susceptible transcript into an exosome/DRN resistant one. To test this, we determined whether the abundance of any of the deletion constructs described in the previous section would remain similar when DRN was inactivated by deleting the *CBC1* gene. As shown in Fig. 3A–B, the abundance of the full-length and most of the deleted constructs was enhanced in a strain where DRN function is depleted (harbors a *cbc1*-Δ allele) except for *SKS1-N*-Δ3, *SKS1-N*-Δ4, and *SKS1-N*-Δ6 transcripts. Note that the abundance of these three deleted messages was already much higher than other deleted messages and did not alter any further in the absence of a functional DRN apparatus (Fig. 3A–B and Table 4).

Furthermore, the abundance of the full-length *SKS1*, *SKS1-N*-Δ2, and *SKS1-N*-Δ5 transcripts was found to be enhanced in both the *cbc1*-Δ and *rrp6*-Δ strains, whereas that of the *SKS1-N*-Δ6 transcript lacking the 202-nt segment harboring the nuclear zip code remains unaltered in these strains (Fig. 4A–B). This finding is thus consistent with the idea that elimination of the 202-nt segment is critical for the nuclear retention and susceptibility to the nuclear exosome/DRN. We also determined the abundance of two arbitrarily chosen messages, *RNA15* and *LYS2*, in all of these yeast strains, none of which revealed any significant alteration in

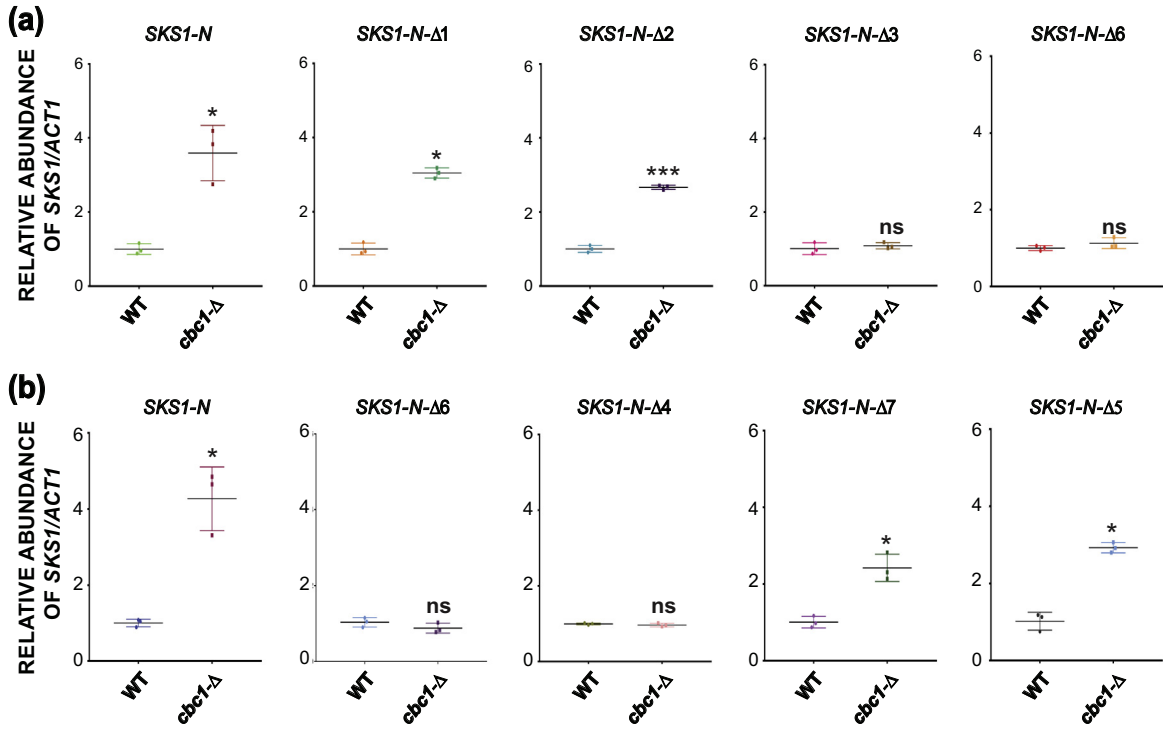

Fig. 3. The *SKS1* nuclear zip code is critical for its susceptibility to the nuclear exosome co-factor, DRN, and its intranuclear decay by DRN component, Cbc1p. Scatter plot revealing the relative levels of native full-length (FL) *SKS1* mRNA (*SKS1-N*) and its deletion versions (*SKS1-N*-Δ1, *SKS1-N*-Δ2, *SKS1-N*-Δ3, and *SKS1-N*-Δ6 are shown in panel A and *SKS1-N*-Δ6, *SKS1-N*-Δ4, *SKS1-N*-Δ7, and *SKS1-N*-Δ5 are shown in panel B) in a normal (yBD-5) and DRN-defective *cbc1*-Δ strain (yBD-6) determined by qRT-PCR analysis using random oligomer-primed cDNA samples and with a primer set encompassing the amplicon R2 (shown in Fig. 1A). *ACT1* RNA was used as the internal loading control for all the experiments. Normalized values of each of the *SKS1* message (either full-length or a specific deleted version) in the wild-type yeast strain were set to 1. The statistical significance of difference reflected in the ranges of *P* values estimated from Student's two-tailed *t* tests for a given pair of test strains for each message is presented with the following symbols, *<0.05, **<0.005, and ***<0.001; ns, not significant.

their steady-state level, thus indicating that they do not undergo any degradation by the nuclear exosome/DRN. As shown in Supplementary Figs. S3–4, the steady-state levels of these two transcripts remained unaltered in the wild-type *cbc1*-Δ and *rrp6*-Δ yeast strains carrying the various *SKS1* deletions. These results strongly indicate that the 202-nt segment encompassing from 825 to 1026 nt of the *SKS1* transcript body harbors a nuclear zip code element, which prompts the full-length and most of the *SKS1* deletion messages to be retained in the nucleus, thereby making them susceptible to the action of the nuclear exosome and DRN.

The "zip code" element is vital for the characteristic nuclear localization of the *SKS1* mRNA

Having shown that the nuclear zip code element is crucial for the intracellular abundance of the *SKS1* mRNA and its susceptibility to the nuclear exosome and DRN machinery, we examined if the alteration of the abundance of the zip code-less *SKS1* and its resistance to the nuclear exosome/DRN is associated with its efficient and rapid nuclear export. We determined the intracellular distribution of *SKS1* mRNA in wild-type yeast strain using the GFP imaging technique [60,83]. In this technique, two plasmids, one carrying a reporter *SKS1-U* chimeric gene and the other harboring a U1A–GFP fusion gene, were used. The reporter plasmid harbors the chimeric *SKS1-U* gene, in which 16 tandem repeat modules of U1A RNA hairpin loop were inserted between the ORF and 3′-UTR of *SKS1* gene (Fig. 5A). The second plasmid carries a U1A–GFP fusion gene that consists of U1A RNA binding protein (does not exist in yeast) fused to GFP placed under the control of *pGAL1* promoter (Fig. 5A). Both of these plasmids were co-transformed in wild-type yeast strain followed by the induction of the U1A–GFP fusion gene by 1% galactose for 50 min at 30 °C and repression by 2% glucose for 90 min. The U1A–GFP fusion protein thus expressed binds to the U1A hairpin loop of either *PGK1-U* or *SKS1-U* (or its deletion constructs) reporter alleles (Fig. 5B), and

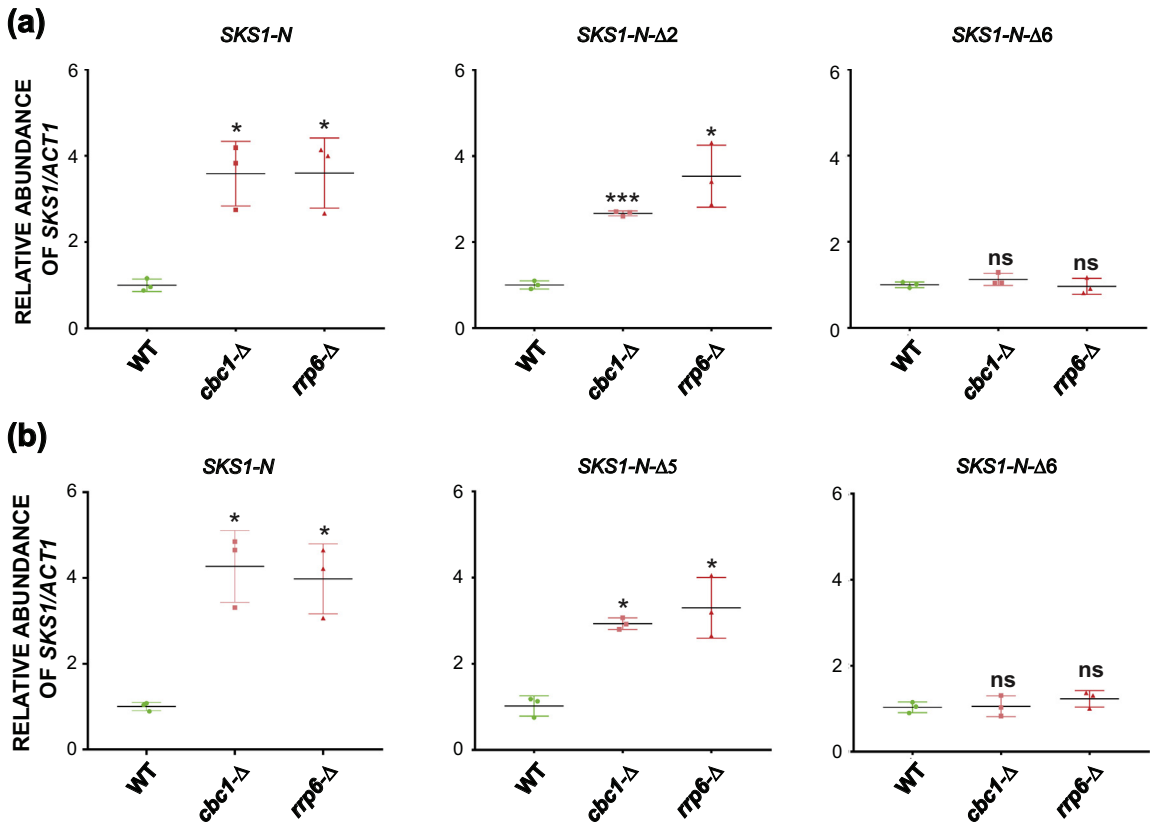

Fig. 4. The *SKS1* nuclear zip code dictates its intra-nuclear decay by the nuclear exosome component, Rrp6p. Scatter plot revealing the relative levels of native full-length (FL) *SKS1* mRNA (*SKS1-N*) and deletion versions (*SKS1-N*-Δ2 and *SKS1-N*-Δ6 are shown in panel A, and *SKS1-N*-Δ5 and *SKS1-N*-Δ6 are shown in panel B) in a normal (yBD-5) DRN-defective *cbc1*-Δ strain (yBD-6) and exosome-defective *rrp6*-Δ strain (yBD-11) as determined by qRT-PCR analysis using random oligomer-primed cDNA samples with a primer set encompassing the amplicon R2 (shown in Fig. 1A). *ACT1* RNA was used as the internal loading control for all the experiments. Normalized values of each of the *SKS1* message (either full-length or a specific deleted version) in the wild-type yeast strain were set to 1. The statistical significance of difference reflected in the ranges of *P* values estimated from Student's two-tailed *t* tests for a given pair of test strains for each message is presented with the following symbols, *<0.05, **<0.005, and ***<0.001; ns, not significant.

the localization of the mRNA-bound GFP signal was determined using live cell confocal imaging. It is worth mentioning here that the GFP signal thus detected specifically represents the distribution of the reporter mRNA and not of just the GFP alone [60]. Using this technique, we first verified the distribution of the *PGK1-U* and full-length *SKS1-U* mRNAs to check the reproducibility of the characteristic cytological distribution patterns of these two messages as described earlier (Fig. 5C) [60]. *PGK1-U* displayed its characteristic cytoplasmic distribution and is largely excluded from the cell nucleus. In contrast, full-length *SKS1-U* message was found to be localized mostly to the nucleus, with the minimal signal detected in the cytoplasm. To rule out the possibility that the insertion of the U1A hairpin element between the *SKS1* ORF and 3′-UTR interfered with its biological property, we asked whether the U1A-inserted *SKS1*, that is, *SKS1-U*, behaves like native full-length *SKS1* as far as its susceptibility to the DRN is concerned. Plasmids harboring either the *SKS1-U* allele or the native *SKS1-N* allele were independently transformed into an *sks1*-Δ and *sks1*-Δ *cbc1*-Δ yeast strains followed by the determination of their abundance in these two strains. First, we compared the relative abundance of the *SKS1-N* transcript (lacking the U loop) and *SKS1-U* (harboring the U loop) transcript in *sks1*-Δ yeast strains (*sks1*-Δ yeast strains transformed either with *SKS1-N* or *SKS1-U* construct) by real-time qRT-PCR method as well as by semi-quantitative RT-PCR (to verify their absolute non-normalized levels). As shown in Supplementary Fig. S5, the relative steady-state levels of both the *SKS1-N* and *SKS1-U* mRNAs are very similar and comparable. Moreover, the abundance of both the *SKS1-N* and *SKS1-U* messages was enhanced by about 3-fold when the *CBC1* gene was disrupted (Fig. 5D). This observation confirmed that the insertion of the U1A element did not alter the

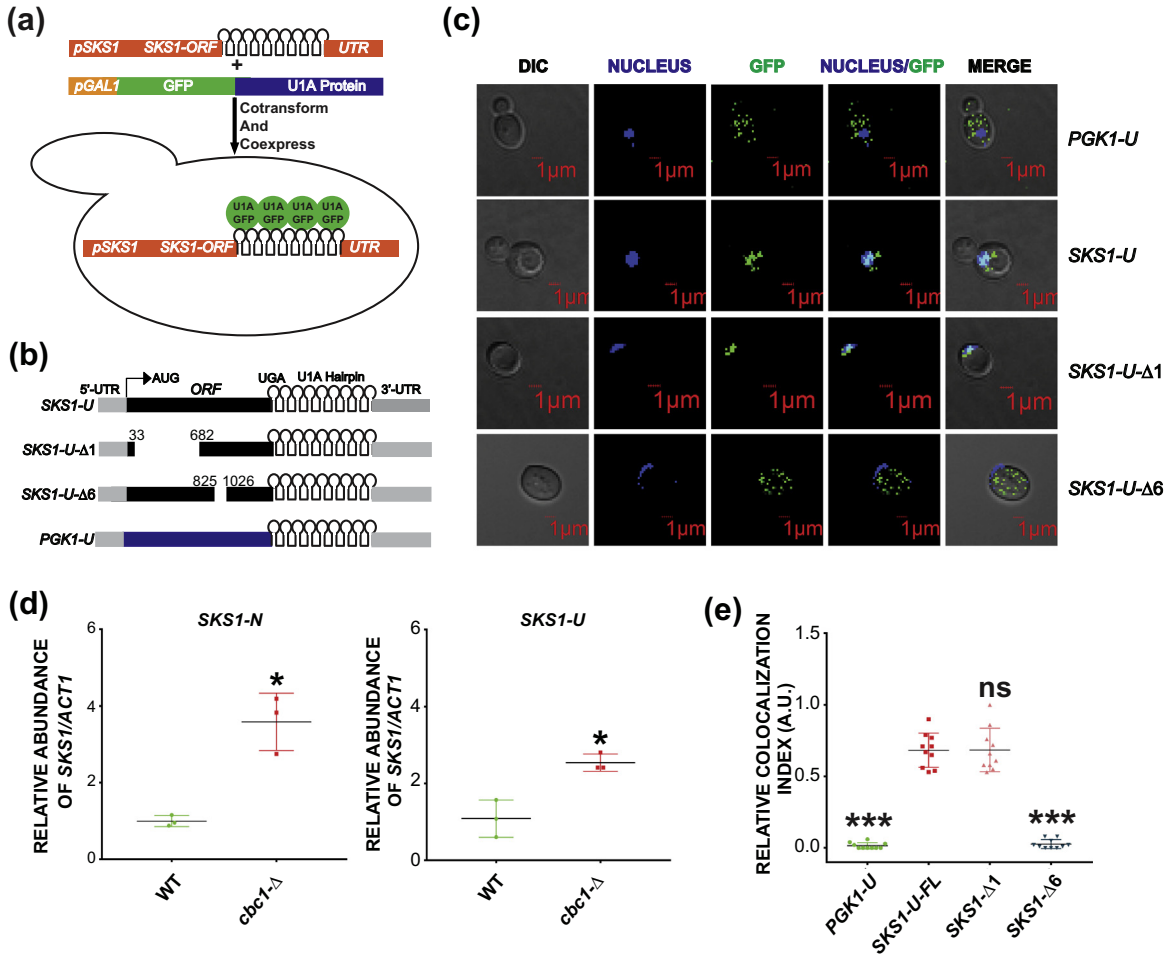

Fig. 5. Nuclear zip code element is responsible for the preferential nuclear distribution of *SKS1* mRNA. (A) Schematic representation of the strategy involved in the GFP imaging technique used to determine the *in situ* distribution of the *SKS1* and other messages. Two different constructs were used in the technique. The first construct consists of sixteen tandem U1A hairpins loops [60] inserted between the translation termination codon and the 3′-UTR of the *SKS1* message, thus creating *SKS1-U* allele expressing the $SKS1^{U1A}$ mRNA. In the second construct, a U1A–GFP fusion is expressed under a $_{P}GAL$ promoter. Note that only the first 94 amino acids of U1A (blue rectangle) were fused in frame to the GFP (green rectangle) [83]. (B) Schematics of various constructs (full-length *SKS1-U*, *PGK1-U*, and selected deleted versions of *SKS1-U*, *SKS1-N-Δ1*, and *SKS1-N-Δ6*) used in this study. Note that the *PGK1-U* construct harbors the 3′-UTR of the *ASH1* and the terminator of the *ADH2* gene (a gift from Dr. Pamela Silver, Harvard University) [83]. (C) *In situ* localization of the *PGK1-U*, *SKS1-U*, *SKS1-N-Δ1*, and *SKS1-N-Δ6* mRNAs decorated with U1A–GFP. Separate cultures of normal wild-type strain (yBD5) harboring each of the RNA reporter construct and U1A–GFP construct were induced with 1% galactose for 50 min followed by the repression with 2% glucose for 90 min. The nucleus was stained by a brief exposure of the culture to 5 μg/ml Hoechst. The images were captured after 50 min from the live cells and processed as described in Materials and Methods. (D) Scatter plot showing the steady-state levels of *SKS1-N* and *SKS1-U* (harboring the U1A hairpin loop) mRNAs in a normal wild-type and *cbc1*-Δ strains ($n = 3$) as determined by qRT-PCR analysis using random oligomer-primed cDNA samples with a primer set encompassing the amplicon R2 (shown in Fig. 1A). Normalized value of each of the *SKS1-N* and *SKS1-U* mRNAs in wild-type strain was set to 1. (E) Scatter plot depicting the co-localization of the Hoechst and the GFP signals from the *PGK1-U*, *SKS1-U (FL)*, *SKS1-N-Δ1*, and *SKS1-N-Δ6* mRNAs. Note that the co-localization index (CI) of two signals found in the yeast strain carrying the reporter *SKS1-U* allele was used as a reference, and the *P* values were calculated concerning this CI obtained in this strain. Co-localization index for nuclear Hoechst and GFP signals was expressed in arbitrary units. Means and standard error of the mean were determined from $n = 10$ cells. CIs (Pearson correlation coefficient, or PCC) were determined as described in the Materials and Methods section. The statistical significance of the difference in values presented in panels D–E as reflected in the ranges of *P* values estimated from Student's two-tailed *t* tests for a given pair of test strains for each message is presented with the following symbols, *<0.05, **<0.005, and ***<0.001; ns, not significant.

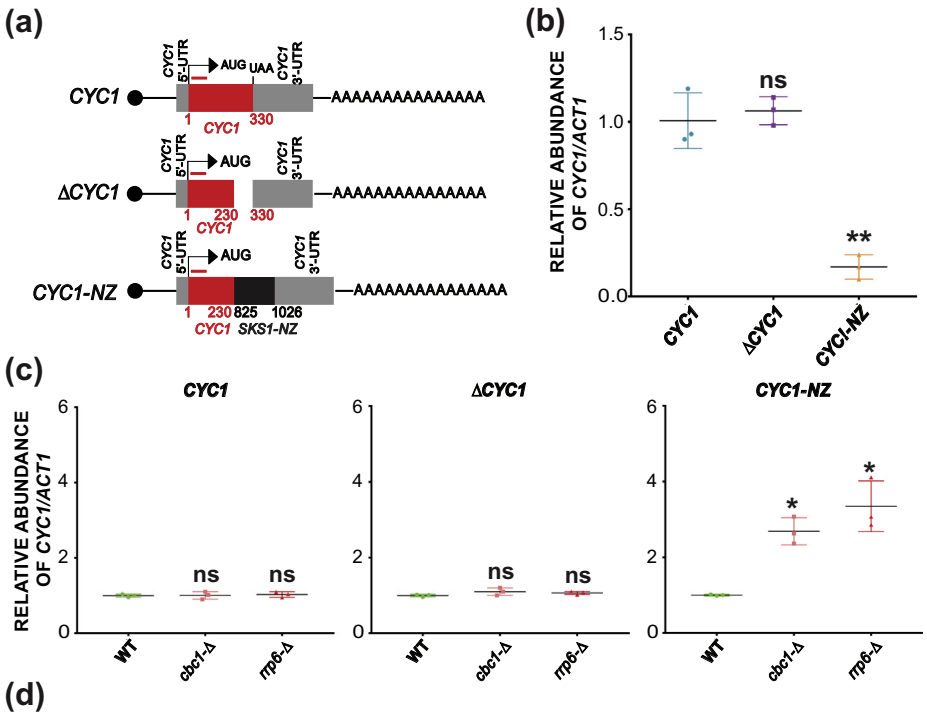

Fig. 6. Incorporation of the *SKS1* nuclear zip code element (*NZ*) into the *CYC1* transcript body transforms this exosome-insensitive mRNA into an exosome-susceptible message. (A) Schematic presentation of the *CYC1*, Δ*CYC1*, and *CYC1-NZ* mRNA used in this study. The *SKS1* nuclear zip code and *CYC1* ORFs are indicated by black and red-filled rectangles, respectively, along with translational start (ATG) and stop (UAA) codons. The gap in the Δ*CYC1* construct indicates the segment, which was deleted from the full-length *CYC1* mRNA. (B) Scatter plot showing the steady-state levels of full-length *CYC1*, Δ*CYC1*, and the *CYC1-NZ* transcripts in a normal wild-type yeast strain ($n = 3$) as determined by qRT-PCR analysis using random oligomer-primed cDNA samples from indicated strains with a primer set encompassing the amplicon C (location shown in Fig. 6A with a red line above the *CYC1* ORF segment). Normalized value of full-length *CYC1* mRNA from was set to 1. (C) Scatter plot showing the steady-state levels of full-length *CYC1*, Δ*CYC1*, and the *CYC1-NZ* transcripts in a wild-type, *cbc1*-Δ, and *rrp6*-Δ yeast strains ($n = 3$) as determined by qRT-PCR analysis using the random oligomer-primed-cDNA samples. Normalized values of each transcript in wild-type cells were set to 1. The statistical significance of difference as reflected in the ranges of *P* values estimated from Student's two-tailed *t* tests for a given pair of test strains for each message is presented with the following symbols, *<0.05, **<0.005, and ***<0.001; ns, not significant. (D) The nucleotide sequence of the 202-nt nuclear zip code (NZ) element (corresponding to the 825–1026 nt of the *SKS1* ORF). Short interspersed pyrimidine (CT)-rich stretches are underlined, and the putative DSR (determinants of selective removal), TGAAAA (110–112), are also indicated in bold. Note that the functionality of none of these elements was validated in this study.

biological property of the *SKS1* message. Therefore, the data obtained from the control experiments (i) reproduced the previous observations made by Kuai *et al.* [60] and (ii) established that the GFP imaging could be employed for studying the cytological distribution of *SKS1* messages and its deleted versions.

We then utilized this imaging technique to ask if eliminating the nuclear zip code can convert nucleus retained *SKS1* mRNA into normally exported transcript. Accordingly, we compared the cytological distribution of the *SKS1-U*-Δ6 reporter message lacking this element to that of *SKS1-U* and *SKS1-U*-Δ1, both carrying this element as negative controls. As shown in Fig. 5C, *SKS1-U*-Δ6 mRNA was found to be largely cytoplasmic, whereas that of the *SKS1-U* and *SKS1-U*-Δ1 is largely nuclear. This suggests that loss of the nuclear zip code in *SKS1-U*-Δ6 mRNA allows its rapid export from the nucleus. Thus, our finding is consistent with the argument that the nuclear zip code slows nuclear export of *SKS1* mRNA.

We also quantified both the Hoechst nuclear DNA stain and GFP signal, and subsequently calculated the co-localization index (CI) as a measure of the nuclear-retained message. As shown in Fig. 5E, the co-localizations of the Hoechst and GFP signals from the full-length *SKS-U* (mean CI ± SEM = 0.683

± 0.038) and *SKS1-U*-Δ1 (mean CI ± SEM = 0.685 ± 0.048) are much higher compared to those of the *PGK1-U* (mean CI ± SEM = 0.015 ± 0.007) and *SKS1-U*-Δ6 (mean CI ± SEM = 0.027 ± 0.010). Thus, these data strongly indicate that the nuclear zip code causes full-length *SKS-U* and *SKS1-U*-Δ1 to be preferentially retained in the nucleus. In contrast, lack of the zip code causes full-length *PGK1-U* and *SKS1-U*-Δ6 to be localized primarily in the cytoplasm. Our collective data lead us to conclude that 202-nt-long segment harboring nuclear zip code element is required for nuclear retention of *SKS1* mRNA.

The "zip code" element can convert a nuclear excluded "typical" mRNA into a nuclear-retained "special" message

Finally, we asked whether the *SKS1* mRNA nuclear zip code is sufficient to convert a normally exported mRNA into one that is retained in the nucleus and degraded by the exosome/DRN. We constructed a chimeric *CYC1-NZ* (*NZ* stands for nuclear zip code) gene by fusing the 230-nt-long 5′-segment from *CYC1* gene to 202-nt-long nuclear zip code element from the *SKS1* transcript (Fig. 6A). The intracellular abundance of a full-length native *CYC1* mRNA lacking its 100-nt 3′-segment (dubbed Δ*CYC1*) and the *CYC1-NZ* chimeric mRNAs was determined. In this and the next experiment, the abundance of the *CYC1-NZ* and the *CYC1* transcript was measured by determining the steady-state levels of a small amplicon present in the 5′-segment of the *CYC1* transcript body by qRT-PCR (location of the amplicon is shown in Fig. 6A as red line above the *CYC1* ORF). As shown in Fig. 6B, the fusion of the 202-nt nuclear zip code of the *SKS1* mRNA reduced the cellular abundance of the *CYC1-NZ* chimeric message to about 15% compared to that of full-length *CYC1* and Δ*CYC1* messages. This finding strongly indicated that the 202-nt-long nuclear zip code is capable of destabilizing a stable message, presumably by retaining within the nucleus.

Next, we addressed if this chimeric transcript displays a susceptibility to the nuclear exosome/DRN just like the native *SKS1*. As presented in Fig. 6C, the abundance of the native *CYC1* and Δ*CYC1* did not change in the yeast strains depleted of either the nuclear exosome component Rrp6p (*rrp6*-Δ) or DRN component Cbc1p (*cbc1*-Δ). In contrast, the abundance of the *CYC1-NZ* transcript was dramatically enhanced in either of the *cbc1*-Δ and *rrp6*-Δ strains that lack the functional DRN or nuclear exosome components, Cbc1p and Rrp6p, respectively. Collectively, these findings strongly argue that fusion of the 202-nt-long nuclear zip code to the 3′-end of the *CYC1* mRNA is sufficient to destabilize the entire transcript, suggesting that it causes nuclear retention of the fused transcript and targets it for the nuclear exosome/DRN.

Discussion

In this study, we present evidence for the existence of a unique *cis*-acting nuclear zip code element in *SKS1* mRNA in *S. cerevisiae*, which prompts its prolonged nuclear retention leading to its intra-nuclear decay by the nuclear exosome/DRN. *SKS1* mRNA encodes a serine/threonine protein kinase that is involved in the regulation and adaptation of the yeast cells in the low glucose medium [71,72]. Notably, this message belongs to a small cohort of mRNAs that are preferentially retained and degraded in the nucleus [60]. We previously postulated that the selective degradation of the *SKS1* mRNA and similar transcripts by the nuclear exosome and DRN plays a key role in regulating their gene expression. Here, we addressed the mechanism of the preferential retention of *SKS1* mRNA in the nucleus and discovered that nuclear retention is caused by the presence of a nuclear zip code element in its transcript body, which in turn results in its susceptibility to DRN. Removal of this sequence alters neither the site nor the length of the transcript's poly(A) tail, indicating that the inferred change in stability is not polyadenylation-dependent (model shown in Fig. 7).

We asked if the nuclear zip code is also required for the susceptibility of the *SKS1* mRNA to the nuclear exosome/DRN. Examination of the steady-state levels of the full-length and various deleted versions of the *SKS1* mRNA in a wild-type, *cbc1*-Δ and *rrp6*-Δ strains revealed that loss of the nuclear zip code from *SKS1* transcripts protects it from degradation by the nuclear exosome/DRN. Moreover, our findings revealed that *SKS1* mRNA is mostly localized in the nucleus, while a construct lacking the nuclear zip code showed a cytoplasmic distribution similar to typical mRNAs (Fig. 5C). In this context, it is noteworthy that none of the deletion constructs were degraded by cytoplasmic NMD. A high steady-state levels of *SKS1*-Δ3, *SKS1*-Δ4, and *SKS1*-Δ6 mRNAs in normal wild-type yeast strain indicate that they are not targeted by the NMD (Fig. 1B and C, Supplementary Fig. S1B and C), although they are exported to the cytoplasm. Furthermore, although the levels of transcripts of the *SKS1*-Δ1, *SKS1*-Δ2, *SKS1*-Δ5, and *SKS1*-Δ7 transcripts are low, these messages are stabilized by the deletions in components of the nuclear mRNA decay systems, such as by *cbc1*-Δ and *rrp6*-Δ (Figs. 3 and 4). This observation clearly indicates that the *SKS1*-Δ1, *SKS1*-Δ2, *SKS1*-Δ5, and *SKS1*-Δ7 transcripts were retained in the nucleus and were actively degraded by the action of the nuclear exosome/DRN decay system. Together, these findings support the view that the nuclear zip code is required for nuclear retention of *SKS1* mRNA. Finally, fusion of the nuclear zip code to the 5′-segment of a heterologous *CYC1* mRNA caused the

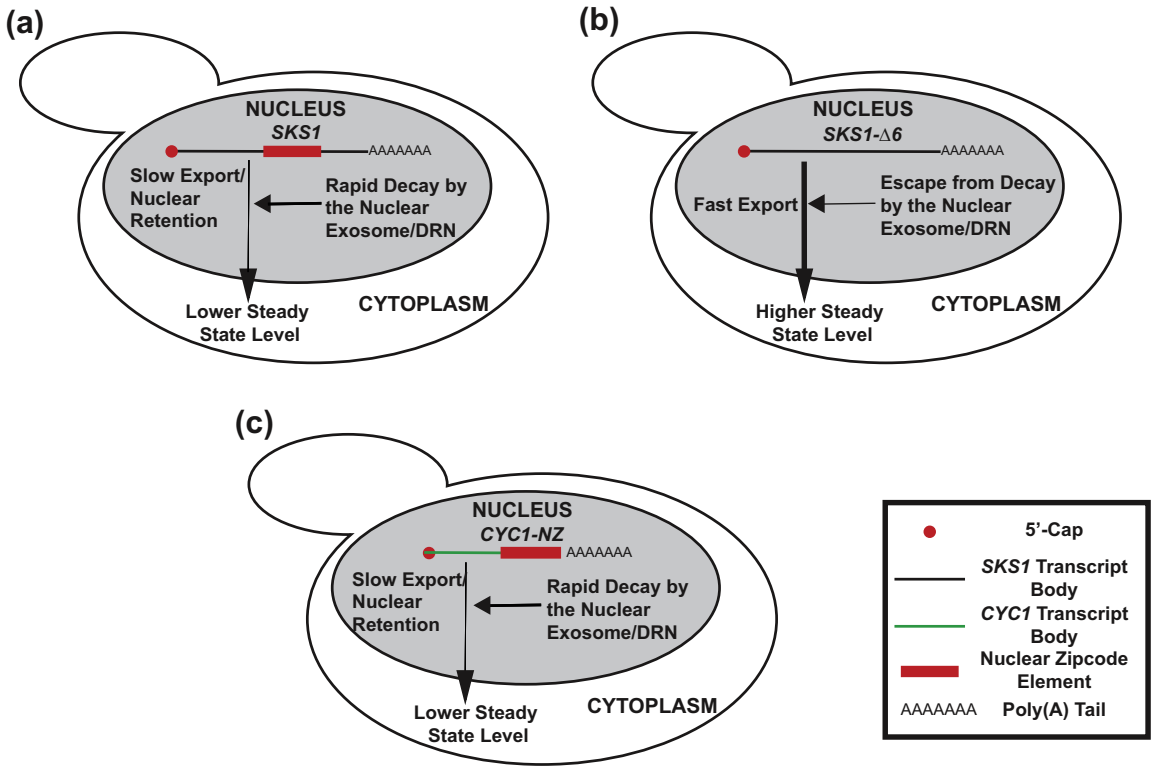

Fig. 7. A model describing the nuclear zip code-dependent preferential retention of *SKS1* (or other) mRNAs in the nucleus of *S. cerevisiae*. (A) *SKS1* mRNA harboring the *cis*-acting nuclear zip code (red box) element is exported very slowly (owing to the propensity of the zip code to retain the message in the nucleus) and is thus subjected to preferential decay activity by the nuclear exosome and DRN. (B) *SKS1-Δ6* mRNA lacking the *cis*-acting nuclear zip code element is exported rapidly and thereby escapes the nuclear exosome/DRN-dependent degradation. (C) Fusion of the nuclear zip code (*NZ*) of the *SKS1* mRNA to the 5′-segment of the *CYC1* mRNA prompts a slow and retarded export of the chimeric message, which is thus subjected to accelerated decay activity by the nuclear exosome and DRN.

chimeric *CYC1-NZ* mRNA to become susceptible to the exosome/DRN (Fig. 6C). We suggest that this susceptibility results from nuclear retention of the chimeric *CYC1-NZ* message, and the result supports the conclusion that the nuclear zip code causes nuclear retention of *SKS1* mRNA, thereby exposing it to the exosome/DRN.

Previously, RNA zip code elements were implicated in the intracellular localization of specific RNAs. The most well-studied and understood example of RNA zip code is provided by *ASH1* mRNA in *S. cerevisiae*. The *ASH1* zip code promotes the transport of this message from the nucleus of the mother cell to the opposite pole of the daughter cells [84–86]. Once *ASH1* mRNA arrives at the opposite pole of the daughter cell, it undergoes translation to produce the Ash1p, which is also asymmetrically and preferentially localized [84–86]. Ash1p prevents the *HO* transcription and thereby inhibits the mating-type switching in the daughter cells [87,88].

Notably, several studies provide examples of nuclear retention of mRNAs in mammals [89–94] (109) as exemplified by a few specific spliced and polyadenylated mRNAs encoding transcription factors, ChREBP, Nlrp6, glucokinase and receptor for glucagon in mouse pancreatic-beta, liver, and gut cell lines, [95]. However, these transcripts were not discerned with any mechanism of nuclear retention [95]. The CTN-RNA, transcribed from the *mCAT2* gene in the mouse, offers another example of the nucleus-retained transcript in the unstressed mouse liver cells with a unique retention mechanism. The gene produces two mRNAs, CTN-RNA, and *mCAT2* mRNA, via the usage of an alternative promoter and poly(A) site [96]. Remarkably, CTN-RNA is retained in nuclear paraspeckles via a mechanism that involves adenosine to inosine editing of the bases in its 3′-UTR, which appears critical for the regulation of the cellular level of *mCAT2* mRNA [96]. During the stress, this element is removed from the CTN-RNA via a site-specific cleavage in the 3′-UTR, thereby releasing the cleaved mRNA from paraspeckles. This cleaved/released mRNA is subsequently exported to the cytoplasm and translated into the *mCAT2* protein, required for rapid uptake of L-arginine for the NO pathway [96].

Although no *cis*-acting nuclear zip code element was implicated in the nuclear retention of the RNAs mentioned above, its involvement in the nuclear retention and decay was demonstrated previously by HIV-1 instability element [97]. This element promotes nuclear retention and decay of the mRNA [94]. More recently, the polypyrimidine tract binding protein (PTB) was shown to relieve the nuclear retention of multiple spliced HIV-1 RNAs and overexpression of PTB promotes nuclear export and cytoplasmic localization [92]. Recently, the Palazzo laboratory has proposed the existence of similar *cis*-element that promotes the nuclear retention and degradation of β-globin mRNA in mammalian cells. The minimal *cis*-element modulating the nuclear retention of this RNA consists of approximately 215 bases [89]. In the fission yeast *Schizosaccharomyces pombe*, "decay-promoting" introns control the abundance of a class of mRNAs by selectively recruiting exosome-specificity factor Mmi1 [91] without promoting their nuclear retention [91]. Interestingly, these decay-promoting introns harbor a common destabilizing motif, DSR (*D*eterminants of *S*elective *R*emoval), which is defined as the hexanucleotide motif U(U/C/G)AAAC [98–100]. Notably, a careful examination of the sequences within the "nuclear zip code" of *SKS1* revealed that at least one such perfect hexanucleotide UGAAAC element spans from 148 to 154 residues of the zip code element (corresponding to 972–978 nt of *SKS1* ORF) (Fig. 6D). Further scrutiny for the presence of potential destabilizing sequences in the 202-nt "zip code" element uncovered stretches of interspersed CU-rich imperfect *Alu*-like elements (Fig. 6D). *Alu*-like CT(CU)-rich sequences are recently implicated in the nuclear retention of long non-coding RNAs and several mRNAs in mammalian cells [101], which potentially enables binding of PTBs. Binding of PTB impacts various processes associated with RNA metabolism [92,97,102,103]. However, the putative functional roles of none of these potentially important elements were validated here. It would certainly be interesting to see whether any of these sequences play any role in the nuclear accumulation and subsequent decay of *SKS1* RNA, which is the subject of our future work.

Although the length of the "nuclear zip code" delineated in this work is 202 nt, it remains unknown if this is the "minimal" zip code element. However, we are in favor of the view that the "minimal" element is shorter than the 202-nt-long segment. Consequently, further dissection of this segment using the similar genetic approach is necessary to identify the minimal nuclear zip code, which is currently underway. Although we did not address the possible mechanism of the nuclear zip code-dependent nuclear retention of the *SKS1* mRNA, we suggest that this element might bind to proteins that block binding of the mRNA to the export receptor Mex67p/Mtr2p. Efforts to identify such factors are currently underway.

Finally, it might be important that a rapid, sharp, and stepwise output is critical for a response to stress stimuli in order for the cell to adapt promptly and to survive under an altered environment (such as in low glucose environment). Therefore, using a post-transcriptional mechanism to control the expression of a subset of genes would be more appropriate and efficient than employing a transcriptional mechanism. In this context, it is worthwhile to recall that *SKS1* encodes a serine/threonine kinase, which plays a role in cellular adjustments to glucose levels. Thus, it may be appropriate for the cells to employ an mRNA degradation and export-based mechanism to control the expression of *SKS1* mRNA.

Materials and Methods

Yeast strains, plasmids, and oligonucleotides

All the strains, plasmids, and oligonucleotides are listed in Tables 1, 2, and 3, respectively.

Nomenclature, yeast strains, media, and yeast genetics

Standard genetic nomenclature is used to designate wild-type alleles, as *CYC1*, *CBC1*, *RRP6*, *SKS1*, and so on; the corresponding disruptants or deletions are designated, for instance, *cbc1*::*URA3*, *cbc1*-$^{\triangle}$, *rrp6*-$^{\triangle}$, *sks1-N*-$^{\triangle}$1, and so on. The protein encoded by a particular gene is denoted, for example, Cbc1p, which is encoded by *CBC1*. Standard YPD, YPG, SC-Leu (leucine omission), and other omission media were used for testing and the growth of yeast [104]. Yeast genetic analysis was carried out by standard procedures as described by Sherman [104].

Construction of various deleted versions *SKS1* Allele and *CYC1-SKS1*-chimeric allele

A series of deleted versions of the *SKS1-N* as well as a selected number of deleted versions of *SKS1-U* allele was constructed by following standard recombinant DNA procedures using either appropriate restriction enzymes or by using reverse PCR-based technology. Similarly, the construction of the *CYC1-NZ* allele was done by fusing the 230-nt segment from the 5′-end of the *CYC1* ORF to the 202-nt nuclear zip code element from the *SKS1* in frame by standard techniques of molecular cloning.

Construction of various yeast strains harboring the various deleted versions *SKS1* allele by two-step gene replacement

Two-step gene replacement was carried out as described before [104]. Various deleted versions of

the *SKS1* alleles in yeast integrating plasmid pRS306 were integrated in the genome in the region containing the *SKS1*$^{+}$ full-length gene. Homologous recombination results in the two copies of the gene, a deleted version and *SKS1*$^{+}$ full-length gene, separated by the plasmid sequence. The full-length copy of the *SKS1*$^{+}$ gene was popped out in the next step by growing the yeast strain in standard 5-fluorouracil medium. The integration of the deleted allele was finally confirmed by genomic PCR using appropriate primer sets.

RNA analyses and determination of steady state of mRNAs

As described earlier [70], the total RNA was isolated by harvesting respective yeast strains. This is followed by the extraction of cell suspension in the presence of glass bead and phenol–chloroform–IAA (25:24:1). The RNA was finally recovered by precipitating it with RNAase-free ethanol.

For cDNA preparation, the RNA samples were treated with one µg RNAase free DNase I (Fermentas Inc.) at 37 °C for 30 min, followed by incubating it with 10 mM EDTA at 65 °C for 10 min. This is followed by cDNA synthesis using iScript Reverse Transcriptase (Biorad) using either random oligodeoxynucleotide primers or oligo-dT primer by incubating it at 25 °C for 5 min (priming), 46 °C for 20 min (reverse transcription), and 95 °C for 1 min (reverse transcriptase inactivation).

End-point semi-quantitative PCR reaction was carried with 1–2 ng cDNA samples using primer sets specific to either *SKS1*, *ACT1*, *RNA15*, and *LYS2* gene, and others, by Taq DNA polymerase (Thermo Fisher Scientific Inc., Waltham, MA, USA). The conditions for individual PCR reactions varied slightly for individual messages. For the data presented in Fig. 1D, 27 cycles of amplification was used, which still lied in the linear range. The PCR products were analyzed on 1% agarose gel, and the signal intensities associated with each band were quantified by the UVI Band software, version 11.0.9.0 (UVIPro Platinum), from three independent biological replicates

Real-Time qPCR analyses were done with 2 ng of cDNA samples. It was used to determine the steady-state levels of *SKS1*, *LYS2*, *RNA15*, and *ACT1.* All the experiments were performed as described previously [70].

Determination of the 5′-UTR, 3′-UTR and length of the poly(A) tails of the SKS1 mRNA and its various deletion versions

5′-UTR of the *SKS1* mRNA was determined by 5′-RACE (Rapid Amplification of cDNA Ends) or "anchored" PCR, which was performed by following the procedure recommended by the manufacturer (Invitrogen Life Technologies 5′ RACE System for Rapid Amplification of cDNA Ends, Version 2.0).

3′-UTR and the length of the poly(A) tail of the *SKS1* mRNA and its all of its deletion versions were determined by LM-PAT assay [74]. Briefly, 200 ng of total RNA was mixed with 20 ng phosphorylated oligo-dT12-18 in 7 µl H_2O and heated to 65 °C for 10 min. The reaction was transferred to 42 °C, and a mixture of 1 µl T4 DNA ligase (10 U/µl), 4 µl 5× iScript Reverse Transcriptase buffer (Biorad), 1 µl RNaseOUTTM (Invitrogen Inc.) (40 U/ml), 2 µl 0.1 M DTT, 1 µl dNTP mix (10 mM each dNTP), 1 µl rATP (10 mM), and 3 µl DEPC H_2O was added, followed by a 30-min incubation at 42 °C. One microliter (200 ng/ml) of oligo(dT)-anchor was then added, and samples were transferred to 12 °C for 2 h. After a 3-min incubation at 42 °C, 2 µl of iScript Reverse Transcriptase (Biorad) (10 U/ml) was added, and the reaction was continued at 25 °C for another 5 min (priming), followed by an incubation at 46 °C for 1 h, and 95 °C for 1 min. Two nanograms of the prepared cDNA sample was used for PCR reaction. Conditions chosen for individual PCR reactions varied slightly depending on the primer used. PCR products were analyzed in a 2% agarose gel.

Confocal microscopy and image processing

Cytological distribution of various RNAs was done by GFP RNA imaging technique as essentially described earlier [83]. The strains were co-transformed with the RNA expression plasmids (*PGK1* allele/*SKS1-U* allele or its deletion constructs *SKS1-U*-Δ1 and *SKS1-U*-Δ6 alleles) and the U1A–GFP expression plasmid. The transformed strain was grown in selective 2% glucose medium overnight followed by transfer into 2% raffinose medium and was further grown to A_{600} of 0.5. Galactose was added (to the final concentration of 1%) at that point to the culture in order to induce the expression of U1A–GFP followed by an inductive growth for 50 min. Cells were then concentrated by centrifugation and were resuspended in selective medium containing 2% glucose followed by growth for an additional 90 min to maximize the GFP signal. Finally, nuclei were stained with Hoechst 33342 stain (5 µg/ml) for 1 min and were washed with glucose medium. Images were obtained by using an OLYMPUS FV10-ASW confocal microscope equipped with HCX PL APO 63X/1.2 NA water immersion objective lens. Image processing was done using OLYMPUS FLUOVIEW Ver.2.0b Viewer software.

In order to determine the co-localization value of the mRNA within the nucleus of *S. cerevisiae* based on captured images, a three-step algorithm is designed in MATLAB, as described below in brevity.

Step 1. Image channel separation

Each image set consists of three images, described as follows:

(a) Image 1—Image of the mRNA distribution (dyed in *green*)
(b) Image 2—Image of the nuclear distribution (dyed in *blue*)
(c) Image 3—Image of the merged mRNA and nuclear distribution from images 1 and 2

Each of these three images of each set was read into the MATLAB script file in the form of a three-dimensional matrix. Subsequently, each image was separated into its respective red, green, and blue channels, where each channel represents one dimension of the 3D Image matrix.

Step 2. **Image thresholding and locating pixels**

An intensity cutoff value was identified and used for thresholding the blue (b_{thresh}) and green (g_{thresh}) channels of the three images. This step is carried out in two hierarchical sub-steps as described below.

A. Determination of percentage of pixel representation in the merged image (image 3)

In order to determine the percentage of pixels being faithfully represented in the merged image 3 formed by the combination of image 1 and image 2, a quantity termed as the representation ratio (RR) is defined such that,

$$RR_g = \frac{\text{Number of Green pixels in image 3 } \left(N_{g_{merge}}\right) \text{ in the green channel}}{\text{Number of Green pixels in image 1} \left(N_{g_{initial}}\right) \text{ in the green channel}}$$

$$RR_b = \frac{\text{Number of blue pixels in image 3 } \left(N_{b_{merge}}\right) \text{ in the blue channel}}{\text{Number of blue pixels in image 2} \left(N_{b_{initial}}\right) \text{ in the blue channel}}$$

The number of pixels in each case is found by detecting the number of matrix cells having intensity values greater than the threshold values b_{thresh} or g_{thresh} for the corresponding channel of the respective images under investigation. If the RR ratios are 100% for the image set under investigation, then it can be interpreted that the merging process has no error and the next sub-step can be carried out.

B. Determination of the number of combined pixels in the merged image (image 3)

In this sub-step, the number of pixels having both blue and green intensities (N_{gb}) in image 3 is determined by using the *find* function for the respective image indices, which have intensity values greater than b_{thresh} and g_{thresh}.

Step 3. **Calculation of co-localization index**

Two co-localization indices are then defined and determined as,

$$CI_{g\_merge} = \frac{\text{Number of combined pixels in image 3 } \left(N_{gb}\right)}{\text{Number of green pixels in image 3 } \left(N_{g_{merge}}\right)}$$

Here, CI_{g_merge} indicates the percentage of mRNA which remains within the nucleus of the yeast cells.

Statistical analyses

The quantitative experiments that are reported in this paper (mRNA steady-state levels, co-localization index) were performed using at least three independent sample size (biological replicates) ($N = 3$). However, for calculating the co-localization index, we used a sample size of 15 cells ($N = 15$). A given yeast strain was grown and treated under the same experimental conditions independently before a given experiment was conducted for each biological replicate. In the case of technical replicate, repetition/analyses of the same biological replicate sample were conducted many times. In order to establish the variability (experimental error) involved in the analysis, a technical replicate was used, which allows the experimenter to set the confidence limits for what are significant data. All the statistical parameters such as mean, standard deviations, *P* values, standard error of the mean, and median were calculated using GraphPad Prism version 7.04 (GraphPad Software Inc., San Diego, CA, USA). *P* values were calculated using Student's two-tailed *t* test (unpaired) using the same program. The values of different statistical parameters (*N*, mean, median, SD, SEM, and *P* value) corresponding to the individual experiments are given in a separate MS Excel File.

Acknowledgments

We gratefully acknowledge Drs. J. Scott Butler (University of Rochester, USA), David Culp (University of Florida, USA), Satarupa Das (Jadavpur University, India), and members of Das laboratory for critically reading the manuscript and useful comments and suggestions. In particular, technical assistance from Mr. Mayukh Banerjea concerning several routine technical procedures is gratefully acknowledged. Kind assistance to use the Confocal Microscope facility of the University of Calcutta from Mr. Shauryabrota Dalui (University of Calcutta, India) is gratefully acknowledged. We are grateful to all the anonymous reviewers for their critical comments and constructive criticisms. We also thank Dr. Deepak Kumar Sinha and Mr. Parijat Biswas, School of Biological Sciences, Indian Association for the

Cultivation of Science, Kolkata, for assistance with the fluorescence microscope facility of Dr. Sinha's laboratory. We also thank Prof. Dhananjay Bhattacharyya, Computer Science Division, Saha Institute of Nuclear Physics, Kolkata, for fruitful discussion.

This investigation was supported by the research grants from the Department of Science and Technology, Government of India (File No. SR/SO/BB-066/2012) to B.D. S.D. is supported by a fellowship from DST-INSPIRE Program of the Ministry of Science and Technology, Government of India (Registration/IVR Number: 201500009398, Inspire Code: IF150640).

Author Contributions: S.B., S.C., and A.B. conducted the experiments. S.D. conceived and conducted the experiments, and wrote the manuscript. B.D. conceived the entire research plan, designed all the experiments, conducted some experiments, directed the entire research program, and organized and wrote the manuscript.

Conflict of Interest: The authors declare no conflict of interest.

Appendix A. Supplementary data

Supplementary data to this article can be found online at https://doi.org/10.1016/j.jmb.2019.07.005.

Received 6 April 2019;
Received in revised form 26 June 2019;
Accepted 1 July 2019
Available online 8 July 2019

Keywords:
DRN;
exosome;
mRNA degradation;
nuclear export;
nuclear zip code

References

[1] P. Bjork, L. Wieslander, Mechanisms of mRNA export, Semin Cell Dev Biol. 32 (2014) 47–54, https://doi.org/10.1016/j.semcdb.2014.04.027S1084-9521(14)00098-6 [pii].

[2] M.B. Fasken, A.H. Corbett, Links between mRNA splicing, mRNA quality control, and intellectual disability, RNA Dis. 3 (2016). doi:e1448 [pii].

[3] D.L. Bentley, The union of transcription and mRNA processing: 20 years of coupling, Rna. 21 (2015) 569–570, https://doi.org/10.1261/rna.050740.115.

[4] G. Bird, N. Fong, J.C. Gatlin, S. Farabaugh, D.L. Bentley, Ribozyme cleavage reveals connections between mRNA release from the site of transcription and pre-mRNA processing, Mol Cell. 20 (2005) 747–758. doi:S1097-2765(05)01769-7 [pii]10.1016/j.molcel.2005.11.009.

[5] R. Luna, H. Gaillard, C. Gonzalez-Aguilera, A. Aguilera, Biogenesis of mRNPs: integrating different processes in the eukaryotic nucleus, Chromosoma. 117 (2008) 319–331, https://doi.org/10.1007/s00412-008-0158-4.

[6] R. Perales, D. Bentley, "Cotranscriptionality": the transcription elongation complex as a nexus for nuclear transactions, Mol Cell. 36 (2009) 178–191, https://doi.org/10.1016/j.molcel.2009.09.018S1097-2765(09)00676-5 [pii].

[7] M. Muller-McNicoll, K.M. Neugebauer, How cells get the message: dynamic assembly and function of mRNA–protein complexes, Nat Rev Genet. 14 (2013) 275–287, https://doi.org/10.1038/nrg3434nrg3434 [pii].

[8] G. Singh, G. Pratt, G.W. Yeo, M.J. Moore, The clothes make the mRNA: past and present trends in mRNP fashion, Annu. Rev. Biochem. 84 (2015) 325–354, https://doi.org/10.1146/annurev-biochem-080111-092106.

[9] N. Kataoka, J. Yong, V.N. Kim, F. Velazquez, R.A. Perkinson, F. Wang, G. Dreyfuss, Pre-mRNA splicing imprints mRNA in the nucleus with a novel RNA-binding protein that persists in the cytoplasm, Mol. Cell. 6 (2000) 673–682.

[10] H. Le Hir, D. Gatfield, E. Izaurralde, M.J. Moore, The exon–exon junction complex provides a binding platform for factors involved in mRNA export and nonsense-mediated mRNA decay, EMBO J. 20 (2001) 4987–4997, https://doi.org/10.1093/emboj/20.17.4987.

[11] E. Wahle, A novel poly(A)-binding protein acts as a specificity factor in the second phase of messenger RNA polyadenylation, Cell. 66 (1991) 759–768.

[12] T. Gonatopoulos-Pournatzis, V.H. Cowling, Cap-binding complex (CBC), Biochem. J. 457 (2014) 231–242, https://doi.org/10.1042/BJ20131214.

[13] A. Kohler, E. Hurt, Exporting RNA from the nucleus to the cytoplasm, Nat Rev Mol Cell Biol. 8 (2007) 761–773. doi:nrm2255 [pii]10.1038/nrm2255.

[14] P. Vinciguerra, F. Stutz, mRNA export: an assembly line from genes to nuclear pores, Curr Opin Cell Biol. 16 (2004) 285–292, https://doi.org/10.1016/j.ceb.2004.03.013S0955067404000511 [pii].

[15] M.J. Moore, N.J. Proudfoot, Pre-mRNA processing reaches back to transcription and ahead to translation, Cell. 136 (2009) 688–700, https://doi.org/10.1016/j.cell.2009.02.001S0092-8674(09)00133-0 [pii].

[16] N.J. Proudfoot, A. Furger, M.J. Dye, Integrating mRNA processing with transcription, Cell. 108 (2002) 501–512 doi:S0092867402006177 [pii].

[17] F. Stutz, E. Izaurralde, The interplay of nuclear mRNP assembly, mRNA surveillance and export, Trends Cell Biol. 13 (2003) 319–327 doi:S0962892403001065 [pii].

[18] E.J. Tran, S.R. Wente, Dynamic nuclear pore complexes: life on the edge, Cell. 125 (2006) 1041–1053, https://doi.org/10.1016/j.cell.2006.05.027.

[19] C. Dimaano, K.S. Ullman, Nucleocytoplasmic transport: integrating mRNA production and turnover with export through the nuclear pore, Mol Cell Biol. 24 (2004) 3069–3076.

[20] S. Rodriguez-Navarro, E. Hurt, Linking gene regulation to mRNA production and export, Curr Opin Cell Biol. 23 (2011) 302–309, https://doi.org/10.1016/j.ceb.2010.12.002S0955-0674(10)00215-2 [pii].

[21] S.J. Schnell, J. Ma, W. Yang, Three-dimensional mapping of mRNA export through the nuclear pore complex, Genes (Basel) 5 (2014) 1032–1049, https://doi.org/10.3390/genes5041032.

[22] G. Haimovich, M. Choder, R.H. Singer, T. Trcek, The fate of the messenger is pre-determined: a new model for regulation of gene expression, Biochim Biophys Acta. 1829 (2013) 643–653, https://doi.org/10.1016/j.bbagrm.2013.01.004S1874-9399(13)00008-4 [pii].
[23] T. Maniatis, R. Reed, An extensive network of coupling among gene expression machines, Nature. 416 (2002) 499–506, https://doi.org/10.1038/416499a416499a [pii].
[24] R. Reed, Coupling transcription, splicing and mRNA export, Curr Opin Cell Biol. 15 (2003) 326–331 doi:S0955067403000486 [pii].
[25] K.M. Neugebauer, On the importance of being co-transcriptional, J Cell Sci. 115 (2002) 3865–3871.
[26] S. Buratowski, Progression through the RNA polymerase II CTD cycle, Mol Cell. 36 (2009) 541–546, https://doi.org/10.1016/j.molcel.2009.10.019S1097-2765(09)00784-9 [pii].
[27] Y. Taur, J.B. Xavier, L. Lipuma, C. Ubeda, J. Goldberg, A. Gobourne, Y.J. Lee, K.A. Dubin, N.D. Socci, A. Viale, M.A. Perales, R.R. Jenq, M.R. van den Brink, E.G. Pamer, Intestinal domination and the risk of bacteremia in patients undergoing allogeneic hematopoietic stem cell transplantation, Clin Infect Dis. 55 (2012) 905–914, https://doi.org/10.1093/cid/cis580cis580 [pii].
[28] D.L. Bentley, Coupling mRNA processing with transcription in time and space, Nat. Rev. Genet. 15 (2014) 163–175, https://doi.org/10.1038/nrg3662.
[29] D.L. Bentley, Rules of engagement: co-transcriptional recruitment of pre-mRNA processing factors, Curr Opin Cell Biol 17 (2005) 251–256, https://doi.org/10.1016/j.ceb.2005.04.006.
[30] A. Aguilera, Cotranscriptional mRNP assembly: from the DNA to the nuclear pore, Curr Opin Cell Biol 17 (2005) 242–250, https://doi.org/10.1016/j.ceb.2005.03.001.
[31] R. Reed, H. Cheng, TREX, SR proteins and export of mRNA, Curr Opin Cell Biol 17 (2005) 269–273, https://doi.org/10.1016/j.ceb.2005.04.011.
[32] A.A. Klauer, A. van Hoof, Degradation of mRNAs that lack a stop codon: a decade of nonstop progress, Wiley Interdiscip Rev RNA. 3 (2012) 649–660, https://doi.org/10.1002/wrna.1124.
[33] K. Schmidt, J.S. Butler, Nuclear RNA surveillance: role of TRAMP in controlling exosome specificity, Wiley Interdiscip Rev RNA. 4 (2013) 217–231, https://doi.org/10.1002/wrna.1155.
[34] S. Lykke-Andersen, T.H. Jensen, Nonsense-mediated mRNA decay: an intricate machinery that shapes transcriptomes, Nat Rev Mol Cell Biol. 16 (2015) 665–677, https://doi.org/10.1038/nrm4063nrm4063 [pii].
[35] S. Lykke-Andersen, R. Tomecki, T.H. Jensen, A. Dziembowski, The eukaryotic RNA exosome: same scaffold but variable catalytic subunits, RNA Biol. 8 (2011) 61–66 doi:14237 [pii].
[36] A. Chlebowski, M. Lubas, T.H. Jensen, A. Dziembowski, RNA decay machines: the exosome, Biochim Biophys Acta. 1829 (2013) 552–560, https://doi.org/10.1016/j.bbagrm.2013.01.006S1874-9399(13)00016-3 [pii].
[37] C. Schneider, D. Tollervey, Threading the barrel of the RNA exosome, Trends Biochem Sci. 38 (2013) 485–493, https://doi.org/10.1016/j.tibs.2013.06.013S0968-0004(13)00105-9 [pii].
[38] A.C. Tuck, D. Tollervey, RNA in pieces, Trends Genet. 27 (2011) 422–432, https://doi.org/10.1016/j.tig.2011.06.001S0168-9525(11)00089-8 [pii].
[39] C. Saguez, J.R. Olesen, T.H. Jensen, Formation of export-competent mRNP: escaping nuclear destruction, Curr Opin Cell Biol. 17 (2005) 287–293. doi:S0955-0674(05)00051-7 [pii]10.1016/j.ceb.2005.04.009.
[40] M. Schmid, Controlling nuclear RNA levels (2018)https://doi.org/10.1038/s41576-018-0013-2.
[41] S. Das, B. Das, MRNA quality control pathways in *Saccharomyces cerevisiae*, J. Biosci 38 (2013)https://doi.org/10.1007/s12038-013-9337-4.
[42] M. Schmid, T.H. Jensen, Transcription-associated quality control of mRNP, Biochim Biophys Acta. 1829 (2013) 158–168, https://doi.org/10.1016/j.bbagrm.2012.08.012S1874-9399(12)00155-1 [pii].
[43] M. Schmid, T.H. Jensen, Quality control of mRNP in the nucleus, Chromosoma. 117 (2008) 419–429, https://doi.org/10.1007/s00412-008-0166-4.
[44] C. Kilchert, S. Wittmann, L. Vasiljeva, The regulation and functions of the nuclear RNA exosome complex, Nat Rev Mol Cell Biol. 17 (2016) 227–239, https://doi.org/10.1038/nrm.2015.15nrm.2015.15 [pii].
[45] M.B. Fasken, A.H. Corbett, Mechanisms of nuclear mRNA quality control., RNA Biol. 6 (n.d.) 237–41.
[46] A. Maity, A. Chaudhuri, B. Das, DRN and TRAMP degrade specific and overlapping aberrant mRNAs formed at various stages of mRNP biogenesis in *Saccharomyces cerevisiae*, FEMS Yeast Res. 16 (2016)https://doi.org/10.1093/femsyr/fow088.
[47] D. Libri, K. Dower, J. Boulay, R. Thomsen, M. Rosbash, T. H. Jensen, Interactions between mRNA export commitment, 3′-end quality control, and nuclear degradation, Mol Cell Biol. 22 (2002) 8254–8266.
[48] D. Zenklusen, P. Vinciguerra, J.C. Wyss, F. Stutz, Stable mRNP formation and export require cotranscriptional recruitment of the mRNA export factors Yra1p and Sub2p by Hpr1p, Mol Cell Biol. 22 (2002) 8241–8253.
[49] K. Strasser, S. Masuda, P. Mason, J. Pfannstiel, M. Oppizzi, S. Rodriguez-Navarro, A.G. Rondon, A. Aguilera, K. Struhl, R. Reed, E. Hurt, TREX is a conserved complex coupling transcription with messenger RNA export, Nature. 417 (2002) 304–308, https://doi.org/10.1038/nature746nature746 [pii].
[50] M. Rougemaille, R.K. Gudipati, J.R. Olesen, R. Thomsen, B. Seraphin, D. Libri, T.H. Jensen, Dissecting mechanisms of nuclear mRNA surveillance in THO/sub2 complex mutants, EMBO J. 26 (2007) 2317–2326, https://doi.org/10.1038/sj.emboj.7601669.
[51] J. Assenholt, J. Mouaikel, K.R. Andersen, D.E. Brodersen, D. Libri, T.H. Jensen, Exonucleolysis is required for nuclear mRNA quality control in yeast THO mutants, RNA. 14 (2008) 2305–2313, https://doi.org/10.1261/rna.1108008rna.1108008 [pii].
[52] T.H. Jensen, K. Dower, D. Libri, M. Rosbash, Early formation of mRNP: license for export or quality control? Mol Cell. 11 (2003) 1129–1138 doi:S1097-2765(03)00191-6 [pii].
[53] R. Thomsen, D. Libri, J. Boulay, M. Rosbash, T.H. Jensen, Localization of nuclear retained mRNAs in *Saccharomyces cerevisiae*, RNA. 9 (2003) 1049–1057.
[54] C. Bousquet-Antonelli, C. Presutti, D. Tollervey, Identification of a regulated pathway for nuclear pre-mRNA turnover, Cell. 102 (2000) 765–775 doi:S0092-8674(00)00065-9 [pii].
[55] R.K. Gudipati, Z. Xu, A. Lebreton, B. Seraphin, L.M. Steinmetz, A. Jacquier, D. Libri, Extensive degradation of RNA precursors by the exosome in wild-type cells, Mol Cell. 48 (2012) 409–421, https://doi.org/10.1016/j.molcel.2012.08.018S1097-2765(12)00736-8 [pii].
[56] C. Schneider, G. Kudla, W. Wlotzka, A. Tuck, D. Tollervey, Transcriptome-wide analysis of exosome targets, Mol Cell.

48 (2012) 422–433, https://doi.org/10.1016/j.molcel.2012.08.013S1097-2765(12)00729-0 [pii].
[57] B. Das, Z. Guo, P. Russo, P. Chartrand, F. Sherman, The role of nuclear cap binding protein Cbc1p of yeast in mRNA termination and degradation, Mol. Cell. Biol. 20 (2000) https://doi.org/10.1128/MCB.20.8.2827-2838.2000.
[58] C. Torchet, C. Bousquet-Antonelli, L. Milligan, E. Thompson, J. Kufel, D. Tollervey, Processing of 3′-extended read-through transcripts by the exosome can generate functional mRNAs, Mol Cell. 9 (2002) 1285–1296 doi:S1097276502005440 [pii].
[59] B. Das, S. Das, F. Sherman, Mutant LYS2 mRNAs retained and degraded in the nucleus of *Saccharomyces cerevisiae*, Proc. Natl. Acad. Sci. U. S. A. 103 (2006). doi:https://doi.org/10.1073/pnas.0604562103.
[60] L. Kuai, B. Das, F. Sherman, A nuclear degradation pathway controls the abundance of normal mRNAs in *Saccharomyces cerevisiae*, Proc. Natl. Acad. Sci. U. S. A. 102 (2005)https://doi.org/10.1073/pnas.0506518102.
[61] R. Parker, RNA degradation in *Saccharomyces cerevisiae*, Genetics. 191 (2012) 671–702, https://doi.org/10.1534/genetics.111.137265191/3/671 [pii].
[62] B. Das, J.S. Butler, F. Sherman, Degradation of normal mRNA in the nucleus of *Saccharomyces cerevisiae*, Mol. Cell. Biol. 23 (2003)https://doi.org/10.1128/MCB.23.16.5502-5515.2003.
[63] J.S. Butler, The yin and yang of the exosome, Trends Cell Biol. 12 (2002) 90–96 doi:S0962892401022255 [pii].
[64] Q. Liu, J.C. Greimann, C.D. Lima, Reconstitution, activities, and structure of the eukaryotic RNA exosome, Cell. 127 (2006) 1223–1237, https://doi.org/10.1016/j.cell.2006.10.037.
[65] A. Dziembowski, E. Lorentzen, E. Conti, B. Seraphin, A single subunit, Dis3, is essentially responsible for yeast exosome core activity, Nat Struct Mol Biol. 14 (2007) 15–22, https://doi.org/10.1038/nsmb1184.
[66] D.L. Makino, M. Baumgartner, E. Conti, Crystal structure of an RNA-bound 11-subunit eukaryotic exosome complex, Nature. 495 (2013) 70–75, https://doi.org/10.1038/nature11870nature11870 [pii].
[67] B. Schuch, M. Feigenbutz, D.L. Makino, S. Falk, C. Basquin, P. Mitchell, E. Conti, The exosome-binding factors Rrp6 and Rrp47 form a composite surface for recruiting the Mtr4 helicase, EMBO J. 33 (2014) 2829–2846, https://doi.org/10.15252/embj.201488757embj.201488757 [pii].
[68] F. Halbach, P. Reichelt, M. Rode, E. Conti, The yeast ski complex: crystal structure and RNA channeling to the exosome complex, Cell. 154 (2013) 814–826, https://doi.org/10.1016/j.cell.2013.07.017S0092-8674(13)00888-X [pii].
[69] S.W. Hardwick, B.F. Luisi, Rarely at rest: RNA helicases and their busy contributions to RNA degradation, regulation and quality control, RNA Biol. 10 (2013) 56–70, https://doi.org/10.4161/rna.2227022270 [pii].
[70] S. Das, U. Saha, B. Das, Cbc2p, Upf3p and eIF4G are components of the DRN (degradation of mRNA in the Nucleus) in *Saccharomyces cerevisiae*, FEMS Yeast Res. 14 (2014)https://doi.org/10.1111/1567-1364.12180.
[71] Z. Yang, L.F. Bisson, The SKS1 protein kinase is a multicopy suppressor of the snf3 mutation of *Saccharomyces cerevisiae*, Yeast. 12 (1996) 1407–1419, https://doi.org/10.1002/(SICI)1097-0061(199611)12:14<1407::AID-YEA36>3.0.CO;2-1.
[72] P. Vagnoli, L.F. Bisson, The SKS1 gene of *Saccharomyces cerevisiae* is required for long-term adaptation of snf3 null strains to low glucose, Yeast. 14 (1998) 359–369, https://doi.org/10.1002/(SICI)1097-0061(19980315)14:4<359::AID-YEA227>3.0.CO;2-#.
[73] S.M. Bresson, N.K. Conrad, The human nuclear poly(A)-binding protein promotes RNA hyperadenylation and decay, PLoS Genet. 9 (2013), e1003893. https://doi.org/10.1371/journal.pgen.1003893.
[74] F.J. Sallés, W.G. Richards, S. Strickland, Assaying the polyadenylation state of mRNAs, Methods A Companion to Methods Enzymol. 17 (1999) 38–45, https://doi.org/10.1006/meth.1998.0705.
[75] A.L. Jalkanen, S.J. Coleman, J. Wilusz, Determinants and implications of mRNA poly(A) tail size—does this protein make my tail look big? Semin. Cell Dev. Biol. 34 (2014) 24–32, https://doi.org/10.1016/j.semcdb.2014.05.018.
[76] G.R. Kumar, B.A. Glaunsinger, Nuclear import of cytoplasmic poly(A) binding protein restricts gene expression via hyperadenylation and nuclear retention of mRNA, Mol. Cell. Biol. 30 (2010) 4996–5008, https://doi.org/10.1128/MCB.00600-10.
[77] T.H. Jensen, K. Patricio, T. McCarthy, M. Rosbash, A block to mRNA nuclear export in *S. cerevisiae* leads to hyperadenylation of transcripts that accumulate at the site of transcription, Mol. Cell. 7 (2001) 887–898.
[78] P. Hilleren, R. Parker, Defects in the mRNA export factors Rat7p, Gle1p, Mex67p, and Rat8p cause hyperadenylation during 3′-end formation of nascent transcripts, RNA. 7 (2001) 753–764.
[79] K.T. Burkard, J.S. Butler, A nuclear 3′–5′ exonuclease involved in mRNA degradation interacts with poly(A) polymerase and the hnRNA protein Npl3p, Mol Cell Biol. 20 (2000) 604–616.
[80] C.E. Birse, L. Minvielle-Sebastia, B.A. Lee, W. Keller, N.J. Proudfoot, Coupling termination of transcription to messenger RNA maturation in yeast, Science 280 (80) (1998) 298–301.
[81] S. Beggs, T.C. James, U. Bond, The polyA tail length of yeast histone mRNAs varies during the cell cycle and is influenced by Sen1p and Rrp6p, Nucleic Acids Res. 40 (2012) 2700–2711, https://doi.org/10.1093/nar/gkr1108.
[82] T.H. Beilharz, T. Preiss, Widespread use of poly(A) tail length control to accentuate expression of the yeast transcriptome, Rna. 13 (2007) 982–997, https://doi.org/10.1261/rna.569407.
[83] A.S. Brodsky, P.A. Silver, Pre-mRNA processing factors are required for nuclear export, RNA. 6 (2000) 1737–1749.
[84] M.P. Cosma, Daughter-specific repression of *Saccharomyces cerevisiae* HO: Ash1 is the commander, EMBO Rep. 5 (2004) 953–957, https://doi.org/10.1038/sj.embor.7400251.
[85] R.M. Long, R.H. Singer, X. Meng, I. Gonzalez, K. Nasmyth, R.P. Jansen, Mating type switching in yeast controlled by asymmetric localization of ASH1 mRNA, Science. 277 (1997) 383–387.
[86] P.A. Takizawa, A. Sil, J.R. Swedlow, I. Herskowitz, R.D. Vale, Actin-dependent localization of an RNA encoding a cell-fate determinant in yeast, Nature. 389 (1997) 90–93, https://doi.org/10.1038/38015.
[87] N. Bobola, R.P. Jansen, T.H. Shin, K. Nasmyth, Asymmetric accumulation of Ash1p in postanaphase nuclei depends on a myosin and restricts yeast mating-type switching to mother cells, Cell. 84 (1996) 699–709.
[88] A. Sil, I. Herskowitz, Identification of asymmetrically localized determinant, Ash1p, required for lineage-specific transcription of the yeast HO gene, Cell. 84 (1996) 711–722.

[89] A. Akef, E.S. Lee, A.F. Palazzo, Splicing promotes the nuclear export of β-globin mRNA by overcoming nuclear retention elements, RNA. 21 (2015) 1908–1920, https://doi.org/10.1261/rna.051987.115.

[90] S.M. Bresson, O.V. Hunter, A.C. Hunter, N.K. Conrad, Canonical poly(A) polymerase activity promotes the decay of a wide variety of mammalian nuclear RNAs, PLoS Genet. 11 (2015), e1005610. https://doi.org/10.1371/journal.pgen.1005610.

[91] C. Kilchert, S. Wittmann, M. Passoni, S. Shah, S. Granneman, L. Vasiljeva, Regulation of mRNA levels by decay-promoting introns that recruit the exosome specificity factor Mmi1, Cell Rep. 13 (2015) 2504–2515, https://doi.org/10.1016/j.celrep.2015.11.026.

[92] K.G. Lassen, K.X. Ramyar, J.R. Bailey, Y. Zhou, R.F. Siliciano, Nuclear retention of multiply spliced HIV-1 RNA in resting CD4+ T cells, PLoS Pathog. 2 (2006) 0650–0661, https://doi.org/10.1371/journal.ppat.0020068.

[93] P. Dunscombe, C. Grau, N. Defourny, J. Malicki, J.M. Borras, M. Coffey, M. Bogusz, C. Gasparotto, B. Slotman, Y. Lievens, A. Kokobobo, F. Sedlmayer, E. Slobina, O. De Hertogh, T. Hadjieva, J. Petera, J. Grau Eriksen, J. Jaal, R. Bly, D. Azria, M. Baumann, Z. Takacsi-Nagy, J. Johannson, M. Cunningham, S. Magrini, V. Atkocius, M. Untereiner, M. Pirotta, V. Karadjinovic, S. Levernes, M. Reinfuss, M.L. Trigo, V. Cernea, P. Dubinsky, B. Segedin, J. Lopez Torrecilla, B. Pastoors, R. Taylor, S. Taylor, Guidelines for equipment and staffing of radiotherapy facilities in the European countries: final results of the ESTRO-HERO survey, Radiother Oncol. 112 (2014) 165–177. doi:10.1016/j.radonc.2014.08.032S0167-8140(14)00362-4 [pii].

[94] A. Zolotukhin, D. Michalowski, J. Bear, S.V. Smulevitch, A. M. Traish, R. Peng, J. Patton, I.N. Shatsky, B.K. Felber, PSF acts through the human immunodeficiency virus type 1 mRNA instability elements to regulate virus expression, Mol. Cell. Biol. 23 (2003) 6618–6630, https://doi.org/10.1128/MCB.23.18.6618.

[95] K.B. Halpern, I. Caspi, D. Lemze, E. Elinav, I. Ulitsky, K.B. Halpern, I. Caspi, D. Lemze, M. Levy, S. Landen, E. Elinav, I. Ulitsky, Nuclear retention of mRNA in mammalian tissues report nuclear retention of mRNA in mammalian tissues, Cell Reports (2015) 1–10, https://doi.org/10.1016/j.celrep.2015.11.036.

[96] K.V. Prasanth, S.G. Prasanth, Z. Xuan, S. Hearn, S.M. Freier, C.F. Bennett, M.Q. Zhang, D.L. Spector, Regulating gene expression through RNA nuclear retention, Cell. 123 (2005) 249–263, https://doi.org/10.1016/j.cell.2005.08.033.

[97] M.Z. Stern, S.K. Gupta, M. Salmon-Divon, T. Haham, O. Barda, S. Levi, C. Wachtel, T.W. Nilsen, S. Michaeli, Multiple roles for polypyrimidine tract binding (PTB) proteins in trypanosome RNA metabolism, Rna. 15 (2009) 648–665, https://doi.org/10.1261/rna.1230209.

[98] H.-M. Chen, B. Futcher, J. Leatherwood, The fission yeast RNA binding protein Mmi1 regulates meiotic genes by controlling intron specific splicing and polyadenylation coupled RNA turnover, PLoS One. 6 (2011), e26804. https://doi.org/10.1371/journal.pone.0026804.

[99] Y. Harigaya, H. Tanaka, S. Yamanaka, K. Tanaka, Y. Watanabe, C. Tsutsumi, Y. Chikashige, Y. Hiraoka, A. Yamashita, M. Yamamoto, Selective elimination of messenger RNA prevents an incidence of untimely meiosis, Nature. 442 (2006) 45–50, https://doi.org/10.1038/nature04881.

[100] A. Yamashita, Y. Shichino, H. Tanaka, E. Hiriart, L. Touat-Todeschini, A. Vavasseur, D.-Q. Ding, Y. Hiraoka, A. Verdel, M. Yamamoto, Hexanucleotide motifs mediate recruitment of the RNA elimination machinery to silent meiotic genes, Open Biol. 2 (2012) 120014, https://doi.org/10.1098/rsob.120014.

[101] Y. Lubelsky, I. Ulitsky, Sequences enriched in Alu repeats drive nuclear localization of long RNAs in human cells, Nature. 555 (2018) 107–111, https://doi.org/10.1038/nature25757.

[102] J. Atallah, C.C. Erickson, F. Cecchin, A.M. Dubin, I.H. Law, M.I. Cohen, M.J. Lapage, B.C. Cannon, T.U. Chun, V. Freedenberg, M. Gierdalski, C.I. Berul, Multi-institutional study of implantable defibrillator lead performance in children and young adults: results of the Pediatric Lead Extractability and Survival Evaluation (PLEASE) study, Circulation. 127 (2013) 2393–2402, https://doi.org/10.1161/CIRCULATIONAHA.112.001120CIRCULATIONAHA.112.001120 [pii].

[103] S.A. Mitchell, K.A. Spriggs, M. Bushell, J.R. Evans, M. Stoneley, J.P.C. Le Quesne, R.V. Spriggs, A.E. Willis, Identification of a motif that mediates polypyrimidine tract-binding protein-dependent internal ribosome entry, Genes Dev. 19 (2005) 1556–1571, https://doi.org/10.1101/gad.339105.

[104] F. Sherman, Getting started with yeast, Methods Enzymol. 194 (1991) 3–21.